

## Electrospun ZnO/poly(vinylidene fluoride-trifluoroethylene) scaffolds for lung tissue engineering

Bahareh Azimi<sup>1,2,3</sup>, Mohammad Sajad Sorayani Bafqi<sup>4</sup>, Alessandra Fusco<sup>5</sup>, Claudio Ricci<sup>1,2</sup>,  
Giuseppe Gallone<sup>1</sup>, Roohollah Bagherzadeh<sup>6</sup>, Giovanna Donnarumma<sup>5</sup>, Mohammed Jasim  
Uddin<sup>7</sup>, Masoud Latifi<sup>4</sup>, Andrea Lazzeri<sup>1</sup>, Serena Danti<sup>1,2,\*</sup>

<sup>1</sup>*Department of Civil and Industrial Engineering, University of Pisa, Largo Lucio Lazzarino,  
56122 Pisa, Italy. Phone: +39 050 2217874, Emails: [b.azimi@ing.unipi.it](mailto:b.azimi@ing.unipi.it),  
[giuseppe.gallone@unipi.it](mailto:giuseppe.gallone@unipi.it), [andrea.lazzeri@unipi.it](mailto:andrea.lazzeri@unipi.it), [serena.danti@unipi.it](mailto:serena.danti@unipi.it)*

<sup>2</sup>*Dept. of Civil and Environmental Engineering, Massachusetts Institute of Technology (MIT),  
Massachusetts Ave. 77, Cambridge, MA, USA. Phone: +1 617-253-710.*

<sup>3</sup>*Interuniversity Consortium of Materials Science and Technology (INSTM), via Giuseppe  
Giusti, 9, 50121 Florence, Italy. Phone: +39 055 23387,1 Email: [clauk8@gmail.com](mailto:clauk8@gmail.com),*

<sup>4</sup>*Department of Textile Engineering, Amirkabir University of Technology, 350 Hafez Ave.,  
Valiasr Square, 15875-4413 Tehran, Iran. Phone: +98 2164542636, Emails:  
[s.sorayani@aut.ac.ir](mailto:s.sorayani@aut.ac.ir), [latifi@aut.ac.ir](mailto:latifi@aut.ac.ir)*

<sup>5</sup>*Department of Experimental Medicine, University of Campania "Luigi Vanvitelli", via Santa  
Maria di Costantinopoli 16, 80138 Naples, Italy. Phone: +39 081 5665935, Emails:  
[alessandra.fusco@unicampania.it](mailto:alessandra.fusco@unicampania.it), [giovanna.donnarumma@unicampania.it](mailto:giovanna.donnarumma@unicampania.it)*

<sup>6</sup>*Institute for Advanced Textile Materials and Technologies (ATMT), Amirkabir University of  
Technology, 350 Hafez Ave., Valiasr Square, 15875-4413 Tehran, Iran. Phone: +98  
2166498038, Email: [bagherzadeh\\_r@aut.ac.ir](mailto:bagherzadeh_r@aut.ac.ir)*

<sup>7</sup>*Department of Chemistry, Photonics and Energy Research Laboratory, University of Texas  
Rio Grande Valley, 1201 W University Dr., Edinburg, TX 78539, USA. Phone: +1-956-665-  
7462, Email: [mohammed.uddin@utrgv.edu](mailto:mohammed.uddin@utrgv.edu)*

- Correspondence to: [serena.danti@unipi.it](mailto:serena.danti@unipi.it)

## Abstract

Due to the morbidity and lethality of pulmonary diseases, new biomaterials and scaffolds are needed to support the regeneration of lung tissues, while ideally providing protective effects against inflammation and microbial aggression. In this study, we investigated the potential of nanocomposites of poly(vinylidene fluoride-co-trifluoroethylene) [P(VDF-TrFE)] incorporating zinc oxide (ZnO), in the form of electrospun fiber meshes for lung tissue engineering. We focused on their anti-inflammatory, antimicrobial and mechano-electrical character according to different fiber mesh textures (i.e., collected at 500 rpm and 4000 rpm) and compositions: (0/100) and (20/80) w/w% ZnO/P(VDF-TrFE), plain and composite, respectively. The scaffolds were characterized in terms of morphological, physico-chemical, mechanical and piezoelectric properties, as well as biological response of A549 alveolar epithelial cells in presence of lung infecting bacteria. By virtue of ZnO, the composite scaffolds showed a strong anti-inflammatory response in A549 cells, as demonstrated by a significant decrease of interleukin (IL) IL-1 $\alpha$ , IL-6 and IL-8 expression in 6 h. In all the scaffold types, but remarkably in the aligned composite ones, transforming growth factor  $\beta$  (TGF- $\beta$ ) and the antimicrobial peptide human  $\beta$  defensin 2 (HBD-2) were significantly increased. The ZnO/P(VDF-TrFE) electrospun fiber meshes hindered the biofilm formation by *S. aureus* and *P. aeruginosa* and the cell/scaffold constructs were able to impede *S. aureus* adhesion and *S. aureus* and *P. aeruginosa* invasiveness, independently of the scaffold type. The data obtained suggested that the composite scaffolds showed potential for tunable mechanical properties, in the range of alveolar walls and fibers. Finally, we also showed good piezoelectricity, which is a feature found in elastic and collagen fibers, the main extracellular matrix molecules in lungs. The combination of all these properties make ZnO/P(VDF-TrFE) fiber meshes promising for lung repair and regeneration.

**Impact statement**

Airway tissue engineering is still a major challenge and an optimally designed scaffold for this application should fulfill a number of key requirements. To help lung repair and regeneration, this study proposes a non-degradable scaffold, with potential for tuning mechanical properties. This scaffold possesses a strong anti-inflammatory character, is able to hinder microbial infections, sustain epithelial cell growth, and provide physiological signals, like piezoelectricity. The development of such a device could help the treatment of pulmonary deficiency, including the ones induced by inflammatory phenomena, primary and secondary to pathogen infections.

## 1. Introduction

Pulmonary tract illnesses are becoming a global healthcare challenge in this century. Tens of millions of people suffer from lung disease in the U.S. and similar rates have been observed in Europe and Asia. Several environmental factors, such as tobacco consumption, air pollution, infections by bacteria and viruses (the latter, SARS-CoV-2), as well as genetic factors, produce structural alterations in our lungs and immune overreactions resulting in acute or chronic conditions (i.e., fibrosis, obstruction and cancer), which overall induce respiratory deficiency with prevalence in the elderly [1]. Some theories have been formulated to explain the origin and perpetuation of inflammatory response in the airways with aging. The main theories point out: (1) the senescence of the innate immune cells and other cells, and/or (2) the possible translocation of bacteria and microbial molecules along the gut-liver-lung axis [2]. The latter theory takes into account the high concentration of pro-inflammatory cytokines, such as interleukin 1 $\beta$  (IL-1 $\beta$ ), IL-6 and tumor necrosis factor  $\alpha$  (TNF- $\alpha$ ), as a result of bacterial debris and lipopolysaccharides passing through gaps being formed at the intestinal epithelial barrier and reaching the liver and the lungs via the lymphatic system [2]. The abovementioned pro-inflammatory mediators are able to activate the enzyme myosin light chain kinase (MLCK), usually silent in epithelial and endothelial cells, which, in the lungs, can lead to pulmonary edema.

In order to provide better outcomes in pulmonary disease treatments, tissue engineering approaches are under development, aimed to regenerate the whole organ, its parts or components [1]. The overall idea is to obtain tissue-engineered substitutes that can be grafted into body for long term, thus being able to simulate the structure and function of lung tissues [3]. In a tissue engineering approach, biomaterial scaffold, cells and stimuli, represent the three fundamental pillars. The scaffolds enable physical cues for three-dimensional (3D) adhesion and growth of cells, which can be present *in vivo*, but may need stimulatory cues to enable their function. Until now, the most commonly studied scaffolds for lung regeneration are based on biological tissues, such as decellularized lungs from different animal species, while a few attempts have developed biological (e.g., collagen, fibronectin) hydrogels or sponges made of synthetic polymers [e.g., polylactide (PLA), poly(lactic-co-glycolic acid) (PLGA)] combined with polysaccharides (e.g. agarose, gelatin) [1]. The role of the scaffold can be manifold, not only structural. As an example, smart

biomaterials can inherently provide a stimulatory microenvironment. This is the case of piezoelectric polymers, which have recently found many applications in the human body, including tissue engineering scaffolds, sensors and energy harvesters [4]. Piezoelectric materials perpetually transform mechanical energy into electric signals (i.e., a transient polarization) and *vice versa* thanks to their crystalline structure characteristics. Among them, some ceramics (e.g., barium titanate, lithium niobate, zinc oxide), and some (co)polymers, mainly belonging to the polyvinylidene fluoride (PVDF) family, possess high piezoelectric properties [4].

In the human body, a number of molecules and tissues have been recognized to possess bioelectric and piezoelectric properties, such as connective tissues (e.g., bone, cartilage, tendons, skin), by virtue of collagen and elastin [5]. Asymmetry found in most biological molecules is at the origin of the piezoelectric effect in the organic matter [6]. Indeed, reorientation occurring in biological macromolecules under stress create a transient change in dipole moments [7]. As a consequence, piezoelectricity has been successfully used in some biomedical applications, such as in amino acid inspired-biomaterials for biosensors [8]. It has been hypothesized that regeneration or healing of electrically-sensitive tissues may be triggered by mechano-electric bio-signals. As such, tissues in which bioelectricity driven by mechanical forces has a pivotal role, may potentially benefit from the application of piezoelectric materials to support their function. Elastin is a key extracellular matrix (ECM) component, present in several tissues, and accounts for approximately 30% in weight percentage (w%) of dry weight in the lungs. As hundred million cycles of inhalation and exhalation occur in a lifetime, elastin deformation consistently enables transient electric charge generation in pulmonary tissues, thus suggesting a possible physiological significance of piezoelectricity in lung tissue engineering [9].

Due to the great complexity of the lung architecture, made up by more than forty specialized cell types, a progress toward an engineered lung could be accomplished through the development of effective and functional scaffolds [10]. Many other advances are still needed in designing pulmonary scaffolds, including better control of ultrastructure and porosity, improved strength and elasticity, as well as enhanced bioactivity to promote cell function [11]. Vascularization has often been reported to be the limiting factor in

engineering complex three-dimensional (3D) tissues, such as lungs [10]. Lung must be capable of exchanging sufficient gas between the airway and vascular compartments. Supporting gas exchange with proper capillary-alveolar distribution is one of the specific requirements for engineering the lung parenchyma [10]. The partial pressure of oxygen in the pulmonary vein should be at least 50 mm Hg, a minimal level that would be indicative of pulmonary function and compatible with survival [12]. Several strategies have been employed to improve the oxygenation of cells grown *in vitro*, including the addition of perfluorocarbons and the bubbling of oxygen through the culture media [10]. It is thus hypothesized that the piezoelectric charge generation during cycles of inhalation and exhalation could play a role in binding of oxygen to hemoglobin, and the polarity switching can help to damp out the possible sudden increase in air pressure [9].

In addition to the flows from the vasculature, the mechanical environment of the 3D construct must be taken into account. In fact, the pulmonary tissue has a sophisticated mechanical environment, which is constantly distended and relaxed. Thus, polymeric structures used to engineer the lung must be capable of a large elastic recovery in order to withstand such repeated deformations. Complex mechanical environment and vasculature of the lung may eventually require the development of smart composite scaffolds formed from more than one material to provide all of the above scaffold requirements [11].

Even though the piezoelectric effect in lung tissues has been demonstrated, to the best of our knowledge, its physiologic significance in lung tissue engineering has not yet been studied. In addition, bioactive scaffolds able to modulate the inflammatory immune response and provide antibacterial activity have not currently been addressed.

In this study, we designed, fabricated and characterized bioactive electrospun piezoelectric scaffolds based on poly(vinylidene fluoride-co-trifluoroethylene) [P(VDF-TrFE)] as candidates for lung tissue engineering. ZnO nanoparticles were incorporated inside the fibers as antimicrobial agents and different fabrication parameters were investigated to improve the piezoelectric, antimicrobial and specific immunomodulatory properties of the composite scaffolds. Such non-biodegradable (i.e., permanent) scaffolds were designed to perpetually resemble the piezoelectric and elastic properties of the main fibrillar component (i.e., elastin) of the pulmonary ECM without releasing the embedded ZnO nanoparticles, thus controlling potential cytotoxic effects. The fabricated ZnO/P(VDF-TrFE)

scaffolds were tested using A549 human lung adenocarcinoma cell line, which presents type II alveolar epithelium morphology. Specifically, both direct and indirect antimicrobial effects of these scaffold were evaluated, the former against *S. aureus* and *P. aeruginosa*, even in the presence of A549 cells. We demonstrated that electrospun ZnO/P(VDF-TrFE) fiber meshes possess good mechanical and piezoelectric characteristics, sufficient cytocompatibility, as well as high immunomodulatory and antibacterial properties, which may be useful for pulmonary illnesses.

The successful development of smart micro/nanostructured scaffolds provided with specific biomimetic, immunomodulatory and antibacterial properties for lung tissue engineering can potentially contribute to the development of new devices for the treatment of pulmonary diseases.

## **2. Materials and Methods**

### **2.1. Materials**

P(VDF-TrFE) powder (70:30 mol %) was purchased from Piezotech Arkema (Pierre-Benite, France) and methyl ethyl ketone (MEK; code 109708) was obtained from Merck (Darmstadt, Germany). ZnO nanopowder with an average particle size of ~15 nm was purchased from US Research Nanomaterials Inc. (Houston, TX, USA). A549 (CCL-185) human lung adenocarcinoma cell line, *S. aureus* (ATCC 6538) and *P. aeruginosa* (ATCC 9027) bacteria, as well their culture substrates [Tryptic-Soy (TS) agar and Luria-Bertani (LB) agar, respectively] were obtained from ATCC (Manassas, VA, USA). L-glutamine, penicillin, streptomycin, gentamycin sulphate, heat-inactivated fetal bovine serum (FBS), RPMI culture medium, L-glutamine, poly-l-lysine, trypsin, Triton X, absolute ethanol, gelatin (type B, from bovine skin), MgCl<sub>2</sub>, 3(4,5dimethylthiazol2yl)2,5diphenyl tetrazolium bromide (MTT) and crystal violet were purchased from Sigma-Aldrich (Milan, Italy). Phosphate Buffered Saline (PBS, 1×) 4',6-diamidino-2-phenylindole (DAPI) and alamarBlue was purchased from ThermoFisher Scientific (Waltham, MA, USA). Fluconazole was supplied by Fresenius Kabi (Verona, Italy). Neutral buffered formalin was purchased from (Bio-Optica, Milan, Italy). LC Fast Start DNA Master SYBR Green kit was obtained from Roche Applied Science (Euroclone S.p.A., Pero, Italy).

## 2.2. Production of ZnO/P(VDF-TrFE) fiber meshes

To produce plain fiber meshes, a P(VDF-TrFE) solution was prepared through the dissolution of the polymer in MEK at 20% weight/volume percentage (w/v%) at room temperature (RT) under mechanical stirring for about 12 h. The polymeric solution was then loaded into a 10 ml glass syringe, fitted with a blunt tip stainless steel needle (21G×3/4") and placed into a syringe pump (NE-300, New Era Pump Systems, Inc., NY, USA). A 8 cm diameter cylindrical collector (Linari Engineering s.r.l., Pisa, Italy), was placed at a distance of 15 cm from the tip of the needle. The collector had driven spindle along its main axis coupled with a controlled motor; the rotation axis was directed perpendicular to the needle axis and parallel to the ground floor. The ground terminal of a high voltage supply (S1600079 Linari High Voltage; Linari Engineering s.r.l.) was connected to the metal needle while the positive terminal was connected to the collector; a 35 kV voltage was applied.

The polymer solution was injected from a needle in the presence of electric field at a constant flow rate of 0.016 ml·min<sup>-1</sup>. The production of random-to-aligned electrospun fiber meshes was performed by collecting the polymeric jet onto the rotating collector with collector velocities of either 500 rpm or 4000 rpm. All the fabrication steps were performed at RT with 46% relative humidity. The fiber meshes were kept in an oven at 60°C overnight to remove traces of the organic solvent from the fibers.

The same procedure was used to produce the ZnO-loaded P(VDF-TrFE) fiber meshes. For the preparation of the solution, first, the ZnO nanopowder was dispersed in MEK. The suspension was sonicated (Hielscher ultrasonic processor UP 400 S) for 10 min (Cycle: 0.5, Amplitude: 40 in full power (400 W) and at a frequency of 40 kHz). Then, P(VDF-TrFE) was added, and the solution (20 w/v%) was left at RT for 12 h under mechanical stirring to form a homogeneous dispersion. The final concentration of the ZnO was 20% w/w% with respect to P(VDF-TrFE).

## 2.3. Morphological characterization of ZnO/P(VDF-TrFE) fiber meshes

The morphology of the scaffolds was evaluated by scanning electron microscopy (SEM) using a FEI FEG-Quanta 450 instrument (Field Electron and Ion Company, Hillsboro, OR, USA). Energy Dispersive X-ray spectrometry (EDXS) was used to prove the presence of ZnO nanoparticles on the surface of the fibers. The samples were sputter-coated with gold

(Gold Edwards SP150B, England) before analysis. SEM micrographs were acquired at different magnifications to visualize the details of interest. Image-J software (version 1.46 r; <http://imagej.nih.gov>) was used to determine the average fiber diameter by measuring a representative diameter of 100 different fibers acquired from SEM micrographs.

#### 2.4 Pore characterization of the meshes

The gravimetric porosity of the scaffolds was estimated as:

$$\text{Porosity (\%)} = \left(1 - \frac{\rho_{\text{scaffold}}}{\rho_c}\right) \times 100 \quad (1)$$

where  $\rho_{\text{scaffold}}$  is the density of the fabricated scaffolds, measured with a pycnometer (Duran, Germany) using double-distilled water, while  $\rho_c$  is the density of the unprocessed material. For composite samples  $\rho_{\text{raw}}$  was calculated as:

$$\rho_c = (\rho_p * f_p) + (\rho_z + f_z) \quad (2)$$

where  $\rho_p$  is the density of polymer P(VDF-TrFE) (1.8 g/cm<sup>3</sup>),  $f_p$  is the fraction of polymer,  $\rho_z$  is the density of ZnO (0.4 g/cm<sup>3</sup>) and  $f_z$  is the fraction of ZnO.

Size and distribution of the mesh pores were evaluated via image analysis method [12]. Briefly, SEM images ( $n = 3$ ) were selected. By using ImageJ software, the micrographs were changed to binary colors representing the fibers in white and the void in red to be analyzed. SEM micrographs at 500× and 10,000× magnification were used to evaluate pore size in the range of 5-100 μm and 1-5 μm, respectively. The method assumed these scaffolds to be bi-dimensional. In order to estimate the negative spaces, a threshold tool was applied. The numerical values of the selection parameters were set to give the best visual representation retracing the negative spaces between the reticulum of the fibers, by comparison to the original images. The areas of void interspaces were measured by the software. Thereafter, the pore equivalent diameters were calculated assuming the pore sections to be circles (i.e., the pores to be cylinders). Finally, the data were converted from pixels to microns using an automatic scale bar for calibration.

#### 2.5. Physico-chemical characterization of ZnO/P(VDF-TrFE) fiber meshes

Energy-dispersive analyzer-EDS (Bruker, QUANTAX Xflash Detector 6/10) was used for elemental analysis of the samples. The relative fraction of β-phase in the copolymer matrix,  $F(\beta)$ , was determined by Fourier Transform Infrared (FTIR) spectroscopy. The FTIR spectra of the samples were recorded with a Perkin Elmer Spectrum GX spectrometer

10

using a polarized wire grid (Perkin Elmer, Waltham, Massachusetts, USA). The beam, directed orthogonally to the wider specimen surface, was polarized alternatively parallel or orthogonal to the main axis of the fiber. In the case of anisotropic meshes as obtained using the rotating collector, this measurement allows the evaluation of the influence of collector velocity on the P(VDF-TrFE) crystalline phase content of the samples. All the spectra were collected in the mid-IR region ( $500\text{-}1500\text{ cm}^{-1}$ ) using 16 scans. The relative fraction of  $\beta$ -phase was calculated as follows:

$$F(\beta) = \frac{X_{\beta}}{X_{\beta}+X_{\alpha}} = \frac{A_{\beta}}{1.26 A_{\beta}+A_{\alpha}} \quad (3)$$

where  $A_{\alpha}$  and  $A_{\beta}$  correspond to absorption band intensities at  $530\text{ cm}^{-1}$  and  $840\text{ cm}^{-1}$  for  $\alpha$  and  $\beta$  phases, respectively [13].

Differential scanning calorimetry (DSC) (TA Q200, New Castle, DE, USA), was used to determine the Curie temperature ( $T_c$ ), the melting temperature ( $T_m$ ) and the overall crystalline content in the copolymer matrix of electrospun fiber meshes. The Curie temperature is unique to ferroelectric materials like P(VDF-TrFE), in which a ferroelectric to paraelectric state transformation takes place [14, 15]. In DSC, the experiments were performed by applying a heat-cool-heat temperature protocol in the range  $-70^{\circ}\text{C}$  to  $+250^{\circ}\text{C}$  with a heating rate of  $10\text{ }^{\circ}\text{C}\cdot\text{min}^{-1}$  and a cooling rate of  $5\text{ }^{\circ}\text{C}\cdot\text{min}^{-1}$ . The crystallinity of samples was thus calculated using the following relation:

$$X_c(\%) = \frac{H_{fs}}{H_{ft}} \times 100 \quad (4)$$

where  $H_{fs}$  is the measured heat of fusion to obtain the melting of the sample and  $H_{ft}$  is the heat of fusion for 100% crystalline P(VDF-TrFE) ( $91.45\text{ mJ}\cdot\text{mg}^{-1}$ ) [15].

## 2.6. Mechanical characterization of P(VDF-TrFE)/ZnO fiber meshes

The mechanical properties of the scaffolds were characterized by a mechanical tester (INSTRON 5500R) equipped with MERLIN software (INSTRON; Norwood, MA, USA). The load cell had a maximum capacity of 100 N, the crosshead speed was  $5\text{ mm}\cdot\text{min}^{-1}$ , and the gauge length (2 cm) of the electrospun fiber meshes was determined by the gap between the parallel strips of the frame. An approximate cross section area of each mesh was measured using a thickness gauge. Representative meshes were tested and the results of 3

replicates were reported as mean and standard deviation. Dynamic mechanical analysis (DMA) was carried out by means of a Gabo Eplexor 100 N (Gabo Qualimeter Testanlagen GmbH, Ahlden, Germany). The specimens consisted in strips, about 2 cm long, 1 mm thick and 1 cm wide, which were cut from the fiber meshes. Every strip was subjected to step-wise increasing static strains in the range of 1% to 50% and, at each static strain step, two distinct measurements of the complex elastic modulus were recorded at two different superimposed 50 Hz sinusoidal dynamic strains of 0.25% and 0.50% amplitude, respectively.

### **2.7. Piezoelectric characterization of ZnO/P(VDF-TrFE) fiber meshes**

An in-house designed mechanical-electronic evaluation system (called PiezoTester) was used to measure the output voltage of the samples as an important parameter to determine their piezoelectric properties. The function of the equipment has been demonstrated in a previous study [16]. After predetermined loads were applied to the samples, their electric output was measured by an oscilloscope. An electrical shield was used to protect samples from ambient electrical noise. Briefly, this apparatus is able to measure the applied load, which allows the sensitivity value of fiber meshes to be calculated. The sensitivity of the layer is a parameter that determines the ability of the layer to produce electrical output for each unit of the applied load. It is used to normalize sample outputs based on the applied load to compare them with each other. The value of sensitivity is calculated by the following formula:

$$Sensitivity = \frac{Electrical\ output}{Applied\ load}$$

(5)

The system also has the ability to evaluate the piezoelectric properties of devices with different loading frequencies, as described earlier [16]. A 1.0×1.5 cm<sup>2</sup> rectangular specimen of each sample was cut and placed under a cyclic compressive load of 2.12 N amplitude and 5 Hz frequency. The sensitivity of the layer was normalized by the sample thickness, measured by SDL34 Shirley fabric thickness tester and based on ASTM D1777-96 to reduce the effect of thickness on the output voltage..

### **2.8. *In vitro* culture of ZnO/P(VDF-TrFE) fiber meshes**

The cells used in the present study were at passage 57. A549 cells were seeded at  $1 \cdot 10^5$  cells/T-75 flask using a complete culture medium (CM), consisting of RPMI supplemented with 2 mM L-glutamine, 100 IU/ml penicillin, 100  $\mu\text{g/ml}$  streptomycin and 10% FBS and cultured in an incubator set at 37°C and 5% CO<sub>2</sub>/95% humidified air. CM was replaced every 2/3 days until 70% confluence was reached. The scaffolds were sterilized in absolute ethanol for 24 h, and then rinsed with three washes with PBS 1 $\times$  containing 3 $\times$  penicillin/streptomycin/fluconazole for 15 min. A549 cells were trypsinized, counted with a hemocytometer and resuspended at  $1.5 \cdot 10^5$  in 20  $\mu\text{l}$  of sterile-filtered 2% (w/v) aqueous solution of gelatin, then seeded on the plain and composite scaffolds ( $n = 3$ ) and incubated in a 24 well plate for 1 h at 37°C in an incubator. Subsequently, 1 ml of CM was added to each well. CM was changed every 2 or 3 days and the cultures were carried on for 9 days.

### **2.9. Biological characterization of alveolar cell/ZnO/P(VDF-TrFE) fiber constructs**

An assessment of ZnO cytotoxicity in its free form was performed on ZnO nanopowder, in view of a successive comparison *versus* ZnO-loaded fibers. For this purpose, ZnO was suspended in 1  $\text{mg} \cdot \text{ml}^{-1}$  poly-L-lysine/PBS solution to obtain a suspension (5  $\text{mg} \cdot \text{ml}^{-1}$  stock concentration), which was sonicated for 12 h at 20 W using a sonicator (Bransonic sonicator 2510; Marshall Scientific, Hampton, NH, USA). A549 cells were seeded onto 24 well plates and put in contact with either ZnO suspension at 0.64  $\text{mg} \cdot \text{ml}^{-1}$  or ZnO-loaded fibers. The former allowed the cells to be exposed to the amount of ZnO (in the form of a nanopowder) that was loaded in the portion of the composite fibers tested. The alamarBlue® test was performed to disclose cytotoxicity of ZnO nanopowder and ZnO/copolymer composites by measuring the metabolic activity of A549 cells in presence of the materials: specifically, after 24 h with cells in presence of ZnO nanopowder suspension, and on day 1, 3 and 8 with cells grown on the scaffolds. The assay was performed according to the manufacturer's instructions and expressed as percentage of reduced alamarBlue (%ABred). Accordingly, samples ( $n = 3$ ) and negative controls ( $n = 3$ ) were incubated for 3 h at 37 °C with the alamarBlue dye diluted in culture media according to the manufacturer's instructions. At each time-point, 100  $\mu\text{l}$  of supernatant from sample or control was loaded into 96-well plates; then, excess supernatant was removed from the cultures and replaced with fresh culture media. The absorbance (A) of supernatants was

measured at 570 nm and 600 nm wavelengths with a spectrophotometer (Victor 3; PerkinElmer). Finally, %AB<sub>red</sub> was calculated by correlating the absorbance values with the molar extinction coefficients of the dye at the selected wavelengths, as indicated in the protocol provided by the manufacturer.

$$\%AB_{\text{red}} = 100\% \cdot \frac{(117,216 \cdot A_{\text{sample@570 nm}} - 80,586 \cdot A_{\text{sample@600 nm}})}{(155,677 \cdot A_{\text{control@600 nm}} - 14,652 \cdot A_{\text{control@570 nm}})}$$

(5)

At the endpoint, the cell/scaffold constructs were washed twice with PBS 1× and then fixed in 1% (w/v) neutral buffered formalin for 10 min at 4°C. The samples were subsequently washed with 1× PBS and incubated with 10 µg/ml DAPI/1×PBS for 10 min at RT, to detect cell nuclei, and then washed again in 1×PBS. Specimens were observed by an inverted fluorescence microscope equipped with a digital camera (Nikon Eclipse Ti, Amsterdam, The Netherlands). Samples were successively dehydrated in 70% ethanol for 30 min, dehydrated in a vacuum oven at 37°C overnight, mounted on aluminum stubs, sputter-coated with gold (Emitech K550, Quorum Technologies Ltd, UK) and observed via SEM.

## 2.10 Immunomodulatory and antibacterial properties of ZnO/P(VDF-TrFE) fiber meshes

Different assays were carried out to assess the response of A549 lung epithelial cells to the produced scaffolds both in absence and presence of common lung infecting bacteria. These tests included: (1) the inflammatory and indirect antimicrobial response of A549 cells to the scaffolds, (2) the direct antimicrobial effect of the scaffolds towards bacteria and (3) the combined effect of bacteria, A549 cells and scaffolds in terms of (3a) bacterial adhesiveness and (3b) internalization.

(1) *Cell-scaffold interaction.* The inflammatory response and the production of the antimicrobial peptide human β defensin-2 (HBD-2) by A549 cells were evaluated by Real-Time Polymerase Chain Reaction (RT-PCR). The scaffolds were sterilized overnight in absolute ethanol, rinsed 3 times with 1×PBS, placed on the bottom of 96-well plates for cell culture; then A549 cells were seeded on them at  $1 \cdot 10^4$  cells/scaffold. Incubation was carried out for 6 h and 24 h. At each time-point, the mRNA was extracted from the cells and the expression levels of the following molecules were tested: the proinflammatory

cytokines IL-1 $\alpha$ , IL-1 $\beta$ , IL-6, IL-8, and TNF- $\alpha$ , the anti-inflammatory cytokine transforming growth factor  $\beta$  (TGF- $\beta$ ) and HBD-2 were evaluated using RT-PCR. Specifically, at the selected timepoints, the total RNA was isolated and 1  $\mu$ g of it was reverse-transcribed into complementary DNA (cDNA) by random hexamer primers, at 42°C for 45 min, according to the manufacturer's instructions. LC Fast Start DNA Master SYBR Green kit was used as follows: 2  $\mu$ l of cDNA, corresponding to 10 ng of total RNA in 20  $\mu$ l final volume, 3 mM MgCl<sub>2</sub> and 0.5  $\mu$ M sense and antisense primer (Table 1).

(2) *Bacteria-scaffold interaction*. To evaluate the direct antimicrobial properties of the samples, the biofilm assay was performed. Overnight cultures of *Staphylococcus aureus* and *Pseudomonas aeruginosa* were diluted to obtain a concentration of 10<sup>7</sup> colony forming units (CFUs)·ml<sup>-1</sup> each, and aliquots (200  $\mu$ l) of the diluted bacterial suspension with or without scaffolds were placed into 96-well flat-bottom sterile polystyrene microplates and incubated overnight at 37 °C in aerobic conditions. After 24 h, the attached bacteria were washed twice with 200  $\mu$ l of PBS×1 and air-dried for 45 min. The samples were then stained with 200  $\mu$ l of 1% aqueous crystal violet solution for 45 min. The plates were rinsed with 200  $\mu$ l of sterile distilled water to remove excess dye and air-dried. The dye associated with the attached biofilm was dissolved in a solution of 200  $\mu$ l of absolute ethanol, and the MTT assay was performed by measuring OD 570/655 nm absorbance on a microplate reader (Victor 3; PerkinElmer).

(3) *Bacteria-cell-scaffold interaction*. (3a) For adhesiveness assays, semiconfluent monolayers of A549 cells (i.e., 8·10<sup>5</sup> cells per 48-well plate) were grown overnight in CM, washed and infected with exponentially growing numbers of *S. aureus* or *P. aeruginosa* with or without ZnO/P(VDF-TrFE) fiber meshes, at 37°C in 5% CO<sub>2</sub>/95% humidified air incubator for 4 h. At the endpoint, infected cell monolayers were washed 3 times with PBS×1 to remove non-adherent bacteria. Total number of cell-associated bacteria was determined by lysing the monolayers with 0.1% Triton X-100. Solubilized bacterial CFUs were counted by spreading serial dilutions on LB agar plates and incubating at 37°C overnight. Adhesion efficiency was calculated as the ratio of the number of cell-associated bacteria and the number of bacteria used to infect cell monolayers. (3b) In the internalization assay, A549 cells, infected as previously described, were extensively washed and further incubated for 2 h with fresh CM supplemented with gentamicin

sulphate at  $250 \mu\text{g}\cdot\text{ml}^{-1}$  in order to kill extracellular bacteria. Also in this case, at the endpoint, cell monolayers were washed with PBS $\times$ 1, lysed with 0.1% Triton X-10, serially diluted and plated on LB agar to quantify viable intracellular bacteria (CFU $\cdot\text{ml}^{-1}$ ). The efficiency was calculated as the ratio of the number of cell-internalized bacteria and the number of bacteria used to infect the cell monolayers.

### 2.11 Statistical analysis

Statistical analysis was carried out by SPSS (v.21.0 software from IBM) to specify the significant level of different processing parameters. All data were analyzed using a one-way analysis of variance and post hoc tests (Tukey's and Duncan's) for multiple comparisons. Probability ( $p$ ) values  $< 0.05$  were considered as statistically significant differences.

## 3. Results

### 3.1. Morphological and physico-chemical properties of ZnO/P(VDF-TrFE) scaffolds

By using the electrospinning apparatus under the working conditions described in section 2.2, plain (0/100 w/w%) and ZnO loaded (20/80 w/w%) ZnO/P(VDF-TrFE) fibers were obtained with either random or uniaxially aligned orientations, using 500 rpm and 4000 rpm collector velocities (corresponding to  $2.09 \text{ m}\cdot\text{s}^{-1}$  and  $16.75 \text{ m}\cdot\text{s}^{-1}$  tangential velocities,  $v_t$ , respectively) (Figure 1 a-d). Specifically, random fibers collected at 500 rpm are imaged in Figure 1a (plain) and in Figure 1c (composite); aligned fibers collected at 4000 rpm are imaged in Figure 1b (plain) and in Figure 1d (composite).

ZnO nanopowder was found to be made up by nanoparticles, approximately of 100 nm size (Figure 1e), aggregated in submicrometric clusters quite uniformly incorporated in the copolymer, which led to a rough fiber surface in the composite fibers (Figure 1 c,d). Moreover, both plain and nanocomposite fibers showed surface nanoporosity. EDXS results also confirmed the presence of nanoparticles emerging partially at the surface level of the fibers (Figure 2a), as revealed by the chemical elements detected, in particular Zn and O on the area pointed (Figure 2 b,c).

The fiber diameters for the studied typologies are reported in Table 2. Under the same processing conditions, the addition of ZnO led to significantly higher fiber diameters with respect to their plain counterparts, namely,  $2.43 \pm 0.76 \mu\text{m}$  versus  $1.86 \pm 0.48 \mu\text{m}$  for fibers collected at 500 rpm and  $1.62 \pm 0.58 \mu\text{m}$  versus  $1.27 \pm 0.20 \mu\text{m}$  for fibers collected at

4000 rpm. Overall, the higher the collector speed, the lower the fiber diameters for the two compositions.

Table 2 also shows the porosity of different fiber meshes. Under the same processing conditions, the alignment led to significantly lower porosity with respect to the random fibers, namely,  $94\% \pm 1\%$  versus  $85\% \pm 2\%$  for plain fibers, while it has no significant effect on the porosity of 20/80 (w/w%) ZnO/P(VDF-TrFE) fiber meshes namely,  $92\% \pm 5\%$  for random and  $89\% \pm 7\%$  for aligned fibers. The presence of ZnO had no significant effect on the porosity of pure fiber mesh nor 20/80 (w/w%) ZnO/P(VDF-TrFE). Results of pore size and size distribution of different meshes are reported in Figure 3. The outcomes of image analysis showed that for all type of fiber meshes, the highest percentage of pore numbers was detected in the  $\leq 5 \mu\text{m}$  pore class, specifically, 71.6% and 82.7% for 0/100 and 20/80 (w/w%) ZnO/P(VDF-TrFE) fiber meshes produced at 500 rpm collector velocity and 83.3% and 81.5% for 0/100 and 20/80 (w/w%) ZnO/P(VDF-TrFE) fiber meshes produced at 4000 rpm collector velocity. The cumulative percentage of pores in 5-100  $\mu\text{m}$  classes was 28.4% and 17.1% for 0/100 and 20/80 (w/w%) ZnO/P(VDF-TrFE) produced at 500 rpm collector velocity, whereas it was 16.6% and 18.4% for 0/100 and 20/80 (w/w%) ZnO/P(VDF-TrFE) produced at 4000 rpm collector velocity.

FTIR spectra of 0/100 and 20/80 (w/w%) ZnO/P(VDF-TrFE) fiber meshes produced at different collector velocities are reported in Figure 4. Increasing collector velocity caused the increase in the intensity of the crystalline bands representing  $\beta$  phase at ( $846 \text{ cm}^{-1}$ ,  $884 \text{ cm}^{-1}$ ,  $1124 \text{ cm}^{-1}$ ,  $1181 \text{ cm}^{-1}$ ,  $1285 \text{ cm}^{-1}$  and  $1431 \text{ cm}^{-1}$ ) representing  $\beta$  phase of P(VDF-TrFE) [17, 18] (Figure 4 a,b); this occurred in plain and composite scaffolds, but the effect of collector velocity was more pronounced in the plain ones.

The presence of ZnO nanoparticles inside the fibers reduced the intensity of bands associated with the copolymer chain orientation ( $1076 \text{ cm}^{-1}$  and  $1400 \text{ cm}^{-1}$ ) and also the intensity of the crystalline bands representing the  $\beta$  phase in both random (Figure 4c) and aligned (Figure 4d) fiber meshes. As results of DSC and FTIR analyses, the values of  $X_c$  (%) and  $F(\beta)$  (%), calculated according to the equations (1) and (2), respectively, are reported in Table 3. The presence of ZnO reduced polymer crystallinity, while the fiber stretching induced by the rotating collector increased it, thus supporting the FTIR results.

### 3.2. Mechanical and piezoelectric properties of ZnO/P(VDF-TrFE) scaffolds

The stress–strain curves of plain and composite ZnO/P(VDF-TrFE) fiber meshes produced at 500 rpm and 4000 rpm collector velocities are presented in Figure 5 a,b. Specifically, Figure 5a shows the four types of scaffolds within a restricted stress-strain range in which the tensile behavior can simultaneously be appreciated for all of them. The results highlighted the significance of the degree of alignment, with aligned fiber meshes resulting much stiffer (i.e., higher elastic modulus) and in general opposing much higher stresses to deformation than their aligned counterparts, which conversely showed a larger elongation range. The presence of ZnO nanoparticles inside the fibers influenced the mechanical properties of the mesh by reducing the elongation at break in all the mesh types. It was in fact shown that the plain P(VDF-TrFE) fiber meshes had superior mechanical properties than ZnO-loaded ones, when compared at the same alignment degree. In particular, in aligned sample types the yield stress was around 5.6 MPa in plain *versus* 2 MPa in composite fiber meshes, and elastic moduli were 94.8 MPa in plain *versus* 31.0 MPa in composite fiber meshes, respectively. In random sample types, the elongation at break was 779% in plain *versus* 142% in composite fiber meshes, respectively (Figure 5 a,b). The elastic modulus of the random composite scaffold was 9 kPa.

Further investigation of the mechanical behavior in the composite scaffolds was performed by DMA at RT in the static strain range of (1% - 50%) and constant frequency of 50 Hz. The outcomes were presented in the form of storage modulus  $E'$  (Figure 5c) and  $\tan\delta$  (Figure 5d), that is the ratio between the loss and storage moduli, which provides a measure of damping at each static strain. Under these working conditions, aligned ZnO/P(VDF-Tr-Fe) fibrous meshes exhibited higher storage modulus (increasing with static strain in the range 120-185 MPa), compared to randomly oriented fibrous meshes (ranging in 3-12 MPa). The loss tangent  $\tan\delta$  was found to be about 0.12-0.08 for aligned fiber and 0.15-0.08 for random fiber scaffolds over the applied static strains. Such limited loss values highlighted that the materials, and in particular the aligned fibers, had reduced viscous effects.

Piezoelectric properties of plain and composite electrospun fiber meshes produced at collector velocities of 500 rpm and 4000 rpm were evaluated using a piezo-tester. The measured output voltages are reported in Table 4. Increasing collector velocity from 500

rpm up to 4000 rpm almost doubled the output voltage of the plain scaffolds from  $45 \pm 5$  mV to  $80 \pm 1$  mV, respectively. The presence of ZnO nanoparticles inside the fibers *per se* increased the output voltage of the random and aligned scaffolds, so that the increase due to the collector velocity was less pronounced (i.e.,  $80 \pm 1$  mV in random and  $90 \pm 1$  mV in aligned fiber scaffolds).

### 3.3 Biological characterization of alveolar cell/ZnO/P(VDF-TrFE) fiber constructs

Preliminary cytotoxicity tests were performed using the alamarBlue assay on A549 cells in culture after 24 h exposure to free ZnO nanoparticles and (20/80) (w/w%) ZnO/P(VDF-TrFE) composites. This experiment highlighted an 87% drop of the metabolic activity when ZnO was not entrapped in the copolymer. To better understand the cytotoxicity of the composite scaffolds, the alamarBlue® assay was performed on A549 cells grown on the four types of scaffolds for 8 days, including the plain copolymer ones. The outcomes in Figure 6 highlighted that the cell/plain copolymer scaffold constructs had a higher metabolic activity, measured as dye substrate reduction percent, significantly growing with time from  $63\% \pm 10\%$  on day 1 to  $74\% \pm 10\%$  on day 8 in random fiber meshes ( $p < 0.05$ ), and from  $48\% \pm 14\%$  on day 1 to  $64\% \pm 10\%$  on day 8 in aligned fiber meshes ( $p < 0.001$ ). In contrast, the metabolic activity of the cell/composite scaffold constructs had a small reduction in random fiber meshes (from  $46\% \pm 6\%$  on day 1 to  $37\% \pm 9\%$  on day 8;  $p < 0.05$ ) and did not significantly change (from  $36\% \pm 8\%$  on day 1 to  $38\% \pm 15\%$  on day 8;  $p = \text{n.s.}$ ) in aligned fiber meshes. In the last time-point, it was observed that the metabolic activity of the cell/plain scaffold constructs always prevailed over their composite counterparts ( $p < 0.0001$ ), and the highest was in the random fiber plain copolymer scaffold ( $p < 0.05$ ). At the endpoint, the different samples were analyzed under fluorescence microscopy and SEM. DAPI staining showed that the scaffold surfaces were densely covered by nuclei without signs of pyknosis (Figure 7).

The fluorescence micrographs generally reflected the trend observed in the metabolic activity resulting from the alamarBlue assay (Figure 5), being the plain copolymer scaffolds the best densely populated (Figure 7 a,b). However, they also confirmed the presence of regions full of cell nuclei in the composite scaffolds (Figure 7 c,d), which appeared better uniformly distributed in the aligned fiber meshes. The morphology of A549 cells was analyzed via SEM (Figure 8). The epithelial cells were able to cover the scaffold surface,

and in particular the aligned (0/100), random (0/100) and aligned (20/80) fiber meshes were densely covered by cellular layers. Flat polygonal morphology typical of lung alveolar cells could be observed in aligned (20/80) scaffolds (inset in Figure 8d).

### 3.4 Immunomodulatory and antibacterial properties of ZnO/P(VDF-TrFE) fiber meshes

The inflammatory response and the production of the antimicrobial peptide HBD-2 by A549 cells in contact with plain and composite ZnO/P(VDF-TrFE) scaffolds were evaluated via RT-PCR and normalized by plain cells as control. The results are presented in Figure 9 except those obtained for IL-1 $\beta$  and TNF- $\alpha$ , which simply resulted not regulated by these materials and remained to basal levels of expression in A549 cells. It was shown that the composite scaffolds after 6 h of contact induced strong anti-inflammatory activity; in fact, they significantly downregulated the expression of the pro-inflammatory cytokines IL-1 $\alpha$ , IL-6 and IL-8 (Figure 9 a-c), whereas they upregulated the expression of the anti-inflammatory cytokine TGF- $\beta$  (Figure 9d) at the gene level. The downregulation of the ILs by the composite scaffold was opposite to the plain copolymer scaffold's and was observed independently of the fiber morphology, thus ascribable directly to ZnO. In particular, IL-1 $\alpha$  expression was  $-73\% \pm 12\%$  in random and  $-95\% \pm 5\%$  in aligned composite fiber meshes ( $p < 0.001$  towards their plain copolymer counterparts). IL-6 expression was  $-97\% \pm 2\%$  in random and  $-100\% \pm 1\%$  in aligned composite fiber meshes ( $p < 0.001$  towards their plain copolymer counterparts). Finally, IL-8 expression was  $-88\% \pm 3\%$  in random and  $-56\% \pm 4\%$  in aligned composite fiber meshes ( $p < 0.001$  towards 500 rpm and  $p < 0.01$  towards 500 rpm plain copolymer counterparts). The upregulation of TGF- $\beta$  was observed in all the compositions, but it was more pronounced in the composite fiber meshes, both random ( $135\% \pm 15\%$ ) and aligned ( $225\% \pm 25\%$ ) ( $p < 0.001$  and  $p < 0.0001$ , with respect to their plain copolymer counterparts), the latter being the highest expression level among all ( $p < 0.001$ ). The expression of all these cytokines was modulated after 24 h. Aligned composite fiber meshes showed the highest IL-6 downregulation ( $p < 0.001$ ) and TGF- $\beta$  upregulation ( $p < 0.001$ ) after 24 h among all fiber types.

HBD-2 is an antimicrobial peptide expressed by epithelia as an innate immune response. The composite scaffolds enhanced the expression of this gene by A549 cells with respect to cell basal expression level, with an increase of  $73\% \pm 7\%$  in random ( $p < 0.001$  versus

plain copolymer counterpart) and  $190\% \pm 10\%$  in aligned fiber meshes, the latter being the highest expression level among all ( $p < 0.001$ ). Interestingly, an increase with respect to the basal condition was also observed in the aligned plain copolymer fibers, namely  $58\% \pm 8\%$ , with respect to 0% in random fiber scaffolds, even though the effect was maximal in the composite counterpart ( $p < 0.0001$ ).

The ZnO/P(VDF-TrFE) scaffolds were put in contact with *S. aureus* and *P. aeruginosa* for 24 h to test the direct antibacterial activity. All the scaffolds demonstrated to be able to reduce the biofilm formation with slightly better effects on average in aligned fiber scaffolds and towards *S. aureus* species (i.e.,  $-92\% \pm 23\%$  in aligned composite fibers). However, this effect appeared not to be dependent on ZnO presence in the fibers and the results did not show statistically significant differences in all the materials for each pathogen (Figure 10). This could be attributed to the fact that ZnO presence is not on the surface of each fibers which is in contact with the bacteria.

When the bacteria infected the A549 cell/scaffold constructs, all the ZnO/P(VDF-TrFE) fiber meshes provided a significant reduction of the adhesion capacity of *S. aureus* with respect to the A549 cells cultured on plastics (i.e., bi-dimensional, 2D). In particular, both plain and composite random meshes, reduced *S. aureus* adhesion by  $88\% \pm 17\%$  and  $90\% \pm 15\%$ , respectively. A weaker effect was observed when aligned fibers were used with this bacteria, i.e.,  $-50\% \pm 26\%$  and  $-24\% \pm 6\%$ , respectively, the latter being the lowest protective value observed among all ( $p < 0.01$ ). All the scaffolds led to the total disappearance ( $-100\%$ ) of the invasive capacity for *S. aureus* compared to 2D cultures (Figure 11a). In contrast, for *P. aeruginosa* the protective effect was confined only to the invasiveness ( $-100\%$  for all scaffold types) (Figure 11b). On the contrary, the adhesion of *P. aeruginosa* was enhanced up to  $+210\% \pm 26\%$  by the presence of the scaffolds (random plain ones), although only half of the enhancement was observed in the aligned fiber meshes, both plain ( $125\% \pm 22\%$ ) and composite ( $104\% \pm 19\%$ ), the last representing the slowest increase observed ( $p < 0.001$ ). The obtained data showed that these specific properties are definitely more affected by the fiber texture than the presence of ZnO.

#### 4. Discussion

Airway tissue engineering is an extremely complex topic of research, and for this reason it has so far obtained marginal success. A number of key challenges have been identified in

lung tissue engineering, including cell heterogeneity, mechanobiology, vascularization, immunogenicity, among others, and meeting them all in a scaffold is the highest challenge [3]. Due to the morbidity and lethality of pulmonary diseases, new biomaterials and scaffolds are needed to support the regeneration of lung tissues, while ideally providing protective effects against inflammation and microbial aggression [3]. Such regenerative platforms could also be designed with biomimetic cues in order to stimulate endogenous cell proliferation and activity, thus improving tissue function. The current strategies adopted for lung tissue engineering encompass the use of highly porous spongy scaffolds based on decellularized lung tissues, ECM molecules or common bioresorbable polymers, such as PLA and PLGA [1, 3, 10, 11]. However, these approaches do not incorporate specific functional features to prevent bacterial aggression and inflammatory states.

Our study focused on the development of electrospun fiber meshes provided with suitable mechanical and piezoelectric features to resemble the alveolar ECM, and incorporating ZnO nanoceramic as an antimicrobial agent. Since ZnO nanostructures may exert cytotoxic effects [19], we created a composite material with a non-biodegradable copolymer as a matrix, namely P(VDF-TrFE) and ZnO nanoparticles as a filler. Both these materials also possess piezoelectric properties, thus providing a means for investigating the possible usefulness of this property in this context, and a viable path for tailoring it. The underlying idea is to obtain a non-cytotoxic porous and flexible substrate suitable for alveolar epithelial cell adhesion, which can perpetually provide physiological-like, anti-inflammatory and antimicrobial stimuli to the surrounding airway tissue microenvironment. The development of such a device could help the treatment of pulmonary deficiency, including the ones induced by inflammatory phenomena, primary and secondary to pathogen infections.

Due to the chemical strength of the C-F bond, PVDF and its (co)polymers are chemically inert, bio-thermally stable materials. They are approved by Food and Drug Administration (FDA) for some applications, and have also been proposed in tissue engineering for their special properties [4, 20]. Unlike other fluoropolymers, PVDF is soluble in several solvents, and thus is processable via electrospinning, leading to the formation of fibrous meshes [4]. In this study, fibers with diameters ranging in 1.07 – 3.19  $\mu\text{m}$  were obtained, depending on both the material composition and the collector speed used. Increasing collector velocity

reduced fiber diameter, as a consequence of the mechanical stretching provided by the rotating collector [21]. ZnO nanoparticles were added at high concentration [i.e., 20% (w/w%)] to obtain: (1) a significant ZnO bioavailability at the fiber surface, considering the non-biodegradable nature of the copolymer, therefore being able to exploit its bioactive properties; and (2) an appreciable increase of the piezoelectric response in the composite with respect to the plain copolymer due to the particles present also in the bulk. ZnO nanoparticles were well dispersed inside the P(VDF-TrFE) fiber matrix. Their presence led to an increase of mean fiber diameter in composite scaffolds compared to their plain counterparts, and also inducing fiber size heterogeneity, particularly at lower collector velocity (500 rpm). This phenomenon has also been observed in (20/80) (w/w)% LiNbO<sub>3</sub> nanoparticle/P(VDF-TrFE) electrospun fibers in similar conditions using MEK as a solvent, and can be attributed to an increase of the solution viscosity caused by the dispersed nanofiller [22]. The proposed scaffolds aim to resemble some traits of the lung ECM. The main fibrillar components of lung ECM are elastin, collagen types I, III, IV and V, and fibronectin [23]. Elastin fibers are about 100 nm thick, whereas collagen fibers, occurring as a spiral assembly in type I and III fibrils, reach 1-20 μm. Since ultrafine fiber size commonly obtained via electrospinning ranges from a few microns down to tens of nanometers, this technique enables the production of an artificial ECM for tissue engineering applications [24]. The high porosity (overall in 83%-95%), the greatly interconnected pore nature of the nonwoven, as well as the presence of pores (overall in 17%-28%) with diameters higher than the minimum size of capillaries (i.e., 5 μm) is compatible with red blood cell size and can be suitable for microvasculature infiltration, which is expected to reduce the foreign body reaction.

Fluorinated polymers are able to interact with the biological environment, such as with various serum proteins, and in particular PVDF has been reported to attract high levels of fibronectin and hemoglobin [25]. This characteristic may be beneficial for lung tissue engineering, since fibronectin expressed in lung ECM and interaction with hemoglobin are crucial to allow an efficient gas exchange. In our previous work, we have reported that randomly oriented P(VDF-TrFE) electrospun fiber meshes were able to support HUVEC growth [26]. This 3D model was applied to test the protective effect of olive oil leaf (OLE) polyphenols against oxidative stress damage [26]. Gas exchange from/into red blood cells

occurs in the terminal portions of the pulmonary air spaces up to alveolar ducts and alveoli. To reach the red blood cells carrying hemoglobin, oxygen must pass through a set of physical barriers, from alveolar epithelial cell-lining fluid to capillary endothelial cells [27]. Therefore, a reduced diffusion distance and a high surface area are favorable for gas exchange and can be obtained in a porous scaffold able to support both alveolar epithelial cell and endothelial cell types. This study showed that plain P(VDF-TrFE) electrospun scaffolds, both randomly and aligned architectures, supported A549 alveolar epithelial cell adhesion. Even though the metabolic activity of the cells was higher in the random fiber mesh, dense coverage of the scaffold surface was observed via SEM in the aligned fiber counterpart. The response to fiber alignment by epithelial cells can depend on the specific cell type. Yan *et al.* have demonstrated that topographical guidance in keratinocytes and corneal epithelial cells cultured on randomly and uniaxially oriented PLLA fiber scaffolds dealt with cell shape (i.e., polygonal or spindle-like) and cytoskeletal tension as key factors [28]. These authors have also observed a lower cell proliferation in aligned fiber meshes. However, both cell types grew disorderly on randomly oriented fiber scaffolds; in contrast, keratocytes displayed parallel orientation only on the aligned fiber scaffolds. In ZnO/polycaprolactone (PCL) composite fibers, surface roughness changes have been highlighted, from smooth in plain PCL to rough when ZnO fraction was higher than 2% up to 6% (w/w)%, the latter the maximal concentration tested in this study [29]. Under our processing and environmental conditions, in particular at 46% relative humidity and using MEK as a solvent, surface nanoporous fibers were formed in all ZnO/P(VDF-TrFE) samples. Since P(VDF-TrFE) is hydrophobic, at high relative humidity, the surface of the fibers is wetted and water molecules coalesce into water droplets that ultimately leave nanosized indentations on the fiber surface. The presence of ZnO nanoparticles inside the fibers improved water permeability and led to the formation of composite fibers with slightly lower surface porosity [30]. In addition, the semiconductor ZnO led to the reduction of the dielectric constant of the solution, resulting in the instability of the whip and charge density in the Taylor cone, which affected fiber morphology [31].

However, in agreement with Agustine *et al.*, the high content of ZnO (20% w/w%) led to much evident surface roughness [29]. A high surface area as provided by porosity and/or particles on a submicrometric scale can provide a nanotexture suitable for promoting

epithelial cell adhesion [32]. Concerning the effects of the spatial arrangement of the fibers, in our experiments the morphology of A549 alveolar epithelial cells was best maintained in aligned fibers either with and without ZnO filler.

As mentioned above, a mechanical effect on cytoskeletal regulation has been suggested to occur, depending on the fiber orientation [28]. In this respect, uniaxially aligned fibers usually show the highest tensile modulus, since all the stretched fibers contribute to the tensile force. Among all the other types of fluoropolymers, PVDF family is known to have the highest flexural modulus and the shortest elongation [33]. However, these properties can be highly modulated using electrospun meshes, as a function of fiber alignment and composition, namely, (0/100) versus (20/80) w/w% ZnO/P(VDF-TrFE). The decreased tensile behavior observed in the composite fibers strongly suggested that ZnO nanoparticles at 20% (w/w%) acted as defect in the fibers. This is in line with other studies on ZnO/PCL fiber meshes, highlighting a reinforcement effect only up to 1% (w/w%) [29]. ZnO reduced the crystallinity of the copolymer (-4.32% in random and -4.53% in aligned fibers), as shown by DSC analysis and corroborated by FTIR spectra, possibly by sterically interfering with crystallization process in the short time of fiber formation. In the composite fibers, the tensile modulus was 31.0 MPa in the aligned fiber meshes and 9 kPa in the random counterpart. In fact, a higher force is required to create the same strain of strongly anisotropic fibers than isotropic ones. Therefore, aligned fibers have a higher elastic modulus in comparison to the randomly oriented counterparts. The elastic modulus of the alveolar wall has been estimated to range in 4.4-5.9 kPa, while that of the fibers to range in 310-620 kPa [34]. The composite fiber meshes covered this range while showing an elongation at break overcoming 100%, thus near to lung stretchability. Notably, it can be argued that partially aligned fiber meshes, obtainable at intermediate collector velocity in between the 500-4000 rpm range, could exactly comply with the estimated values for elastic modulus of the alveolar wall and will be evaluated in the future. The low and almost constant values of the loss tangent ( $\tan\delta$ ) with increasing static strain, in particular for aligned fibers, indicated that these materials have limited viscous effects and thus they should be able to support multiple cycles of loading while retaining an elastic behavior. Among others, PVDF and its copolymers are hydrophobic materials, capable of attaining a superhydrophobic character for certain micro- and nano-texture, including electrospun

fibers, which help to provide some antimicrobial properties interesting for biomedical and other applications [35]. To further improve the bactericidal properties for water purification, PVDF electrospun membranes have been decorated with electrosprayed ZnO nanoparticles [36]. Several studies indicated that ZnO in small quantity is not toxic by contributing to normal tissue function, and may have beneficial effects in tissue regeneration by boosting angiogenesis, protected by antimicrobial properties exerted by Zn<sup>2+</sup> release [18, 37, 38]. It has also been reported that Zn could enhance the proliferation of smooth muscle cells [38]. These cells are present in the lungs as bronchial and vascular smooth muscle cells [40]. Electrospun ZnO/PCL composites have been firstly studied, showing the capacity of improving fibroblast growth [29]. However, electrospun ZnO/P(VDF-TrFE) fiber meshes have not yet been investigated in tissue regeneration applications, but rather in strain, pressure and temperature sensors [19, 31, 38]. There are several studies assessing that ZnO nanostructures, like nanorods and nanospheres, possess bactericidal properties against *E. coli* and *S. aureus* [31, 38]. We investigated the bactericidal behavior of the ZnO/P(VDF-TrFE) electrospun scaffolds on *S. aureus* and *P. aeruginosa*, two main bacterial responsible for respiratory tract infections by different mechanisms of action. *S. aureus* is gram-positive, while *P. aeruginosa* is gram-negative; both of them can acquire drug-resistance and deeply infect the airways of non-immunocompetent patients in particular upon intubation. Moreover, *S. aureus* can support subsequent *P. aeruginosa* infection, which usually has a poorer prognosis and induces strong immune reactions [41]. All the ZnO/P(VDF-TrFE) fiber composites developed in this study showed capacity of inhibiting biofilm formation by both types of bacteria in 24 h, the most marked effect being detected on *S. aureus* by all the scaffold types. The obtained results, although not statistically significant, are suggestive of a better pronounced effect exerted by aligned fibers, independently of the presence of ZnO. The direct antimicrobial effect was however less strong against *P. aeruginosa*. Upon bacterial infection of A549 cell/scaffold constructs, all the ZnO/P(VDF-TrFE) fiber meshes, and in particular the randomly oriented types, significantly inhibited *S. aureus* adhesion. In contrast, the adhesion of *P. aeruginosa* was enhanced by the presence of the scaffolds (i.e., random plain ones). All the scaffolds led to the complete disappearance (-100%) of the invasive capacity for *S. aureus* and *P. aeruginosa*. The obtained data showed that these

specific properties observed after 24 h did not strictly depend on the presence of ZnO, but more likely on the fiber texture and copolymer chemistry [35]. The lower the particle size (e.g. 4 nm), the higher the ZnO cytotoxicity due to reactive oxygen species (ROS) concentration [19, 38]. Since our composite is non-biodegradable, ZnO nanoparticles are not expected to be released from the copolymer in their primary way of action. We can presumably hypothesize that the clusters of nanoparticles at the fiber surfaces, may contribute to Zn<sup>2+</sup> release, therefore at a slow rate.

A549 cells cultured on the ZnO/P(VDF-TrFE) fibers upregulated the expression of HBD-2 after 6 h, as demonstrated by RT-PCR. The family of  $\beta$ -defensins is composed of small cationic peptides inherently produced by epithelial and other cells, upon microorganism or cytokine induction, which is a part of the innate immunity. HBD-2 is a small antimicrobial peptide, acting as an endogenous antibiotic in the defense against Gram-positive and Gram-negative bacteria, fungi and the envelope of some viruses [41]. Upon culture on the composite scaffolds, A549 cells expressed much higher levels of HBD-2. By analyzing this outcome, a double effect was observed: (1) a specific effect of ZnO, and (2) an effect of fiber orientation, which made the aligned composite fibers outperforming the others with an increase of  $190\% \pm 10\%$  mRNA with respect to the basal condition of these cells in culture after 6 h. This effect was reduced but still significant after 24 h, thus suggesting a prolonged protective effect as the mRNA will be transduced into protein.

Some studies have reported the ability of ZnO to induce pro-inflammatory cytokines, such as TNF- $\alpha$  and IL-12, in a concentration dependent manner [19]. We investigated a panel of immunoregulatory cytokines, including pro- and anti-inflammatory, to assess the response of alveolar epithelial cells to the fabricated scaffolds: specifically IL-1 ( $\alpha$  and  $\beta$ ), IL-6, IL-8, TNF- $\alpha$ , and TGF- $\beta$ . IL-1 $\alpha$  and IL-1 $\beta$  are two forms of IL-1, produced by two different genes, having a structural homology of 30%, but a virtually identical biological activity. IL-1 showed a dose-dependent behavior by promoting local inflammation up to stimulating the synthesis of acute phase proteins inducing cachexia [43]. IL-6, IL-8 and TNF- $\alpha$  are essentially mediators of inflammation in the bronchial epithelium [44]. Finally, TGF- $\beta$  is considered the most powerful anti-inflammatory cytokine, able to modulate negatively almost all the inflammatory responses. It is also involved in up-regulating collagen production (particularly type I and III) and is also a potent inhibitor of metalloproteinases

[45]. Inflammation is thus characterized by interplay between several pro- and anti-inflammatory cytokines over a timescale, and a modulation in their intensity contributes to the resolution of the inflammatory process.

We showed that the (20/80) w/w% ZnO/P(VDF-TrFE) fiber meshes promoted strong anti-inflammatory effects by significantly reducing the expression of the pro-inflammatory cytokines IL-1 $\alpha$ , IL-6 and IL-8, and at the same time rising the expression of the anti-inflammatory cytokine TGF- $\beta$  in A549 alveolar epithelial cells. IL-1 $\beta$  and TNF- $\alpha$  were not modulated by any scaffolds with respect to the basal conditions of these cells. IL-1, IL-6 and TNF- $\alpha$  are involved in pulmonary edema and viral infection [2, 44]. In any case, the inflammatory process is at the basis of pulmonary diseases [46]. We can thus consider the (20/80) w/w% ZnO/P(VDF-TrFE) fiber meshes as promising candidates to reduce the inflammatory pathology under implantation. Moreover, the composite scaffolds showed a significant indirect antimicrobial activity by stimulating and sustaining the expression of HBD-2 gene. Overall, the aligned (20/80) w/w% ZnO/P(VDF-TrFE) fiber meshes accounted for the most significant effects in terms of upregulation of TGF- $\beta$  and HBD-2 genes in these cells. All IL-related effects concerned the presence of ZnO, which reversed the behavior of the same cells on the plain copolymer counterparts. However, the plain copolymer scaffolds demonstrated some capacity of stimulating TGF- $\beta$  and HBD-2 (only in aligned fibers). This finding is suggestive of a mechanobiological effect occurring in epithelial cells, which may depend on several factors, such as different fiber alignment, pore size and shape, and elastic moduli.

PVDF-based polymers have the best piezoelectricity among plastic materials, due to oriented dipoles of hydrogen and fluoride unit cells in the carbon backbone, which form the crystallographic phase  $\beta$  [13]. In P(VDF-TrFE), the formation of  $\beta$ -phase is promoted with respect to the homopolymer, and therefore the piezoelectricity too [4]. A wide range of biological tissues show piezoelectric effects, including bone, muscles, blood vessels and skin, mainly by virtue of fibrillar ECM molecules such as elastin and collagen, thus suggesting piezoelectricity to be an unveiled key property of biological tissues potentially able to drive physiological functions under exogenous and endogenous mechanical forces [5, 6]. Elastin is a network molecule that accounts for approximately 30% of the lung dry weight and the integrity of the elastin fiber is fundamental in maintaining normal lung

function. Lung tissue is also expected to possess strong electromechanical coupling, due to the piezoelectric effect of elastin. Given the about 3800 million cycles of inhalation and exhalation occurring in one's lifetime, it is hypothesized that the piezoelectric charge generation during inhalation and exhalation could play a role in binding oxygen to hemoglobin, and the polarity switching can help damp out the possible sudden increase in air pressure [9]. Even if the piezoelectric effect in lung tissues has been demonstrated [9], to the best of our knowledge, the application of piezoelectric scaffolds for lung tissue engineering has not been explored yet. One of the most applied processes to promote the  $\beta$  phase in piezoelectric polymers is electrospinning. With this technology, the fibers under formation are mechanically stretched due to the tangent velocity of the rotating collector and meanwhile the polymer chains are oriented by the intense electric field [4]. This process is thus particularly suitable to obtain piezoelectric polymer fibers, as it intrinsically combines a mechanical stretching and an electric poling treatment [47]. In fact, PVDF processed into fibers via electrospinning possesses higher piezoelectric coefficients than the non-processed polymer [48]. Moreover, at 20% weight ratio of the nanosized filler with respect to the polymer, Danti *et al.* and Mota *et al.*, showed that  $\text{LiNbO}_3/\text{P}(\text{VDF-TrFE})$  and  $\text{BaTiO}_3/\text{PVDF}$  aligned composite fibers had enhanced piezoelectric effects [22, 48]. In the  $\text{ZnO}/\text{P}(\text{VDF-TrFE})$  fibers produced in this study, the output voltage was tested as a direct proof of piezoelectricity [20, 21]. The highest  $V_{\text{out}}$  (i.e.,  $90 \pm 1$  mV for 2.12 N load) was obtained in the aligned composite fibers. Augustin *et al.* have reported that the electrospun  $\text{ZnO}/\text{P}(\text{VDF-TrFE})$  piezoelectric scaffolds were biocompatible *in vivo* and promoted angiogenesis [49], which supports our proposal for pulmonary applications. A functional study of the piezoelectric effect in a physiologically simulated environment would be performed in the future to demonstrate the efficiency of these and other piezoelectric materials in mimicking the lung ECM microenvironment.

### Conclusions

Airway tissue engineering is still a major challenge and an optimally designed scaffold for this application should fulfill a number of key requirements. We investigated the potential of  $\text{ZnO}/\text{P}(\text{VDF-TrFE})$  electrospun fiber meshes for lung repair or regeneration, focusing on their anti-inflammatory, antimicrobial and mechano-electrical character according to different fiber mesh textures (i.e., collected at 500 rpm and 4000 rpm) and compositions

[(0/100) and (20/80) w/w% ZnO/P(VDF-TrFE)]. The scaffolds were characterized in terms of morphological, physico-chemical, mechanical and piezoelectric properties, as well as biological response of alveolar epithelial and/or bacterial cells. We showed that by virtue of the ZnO nanofiller, the composite fibers demonstrated strong anti-inflammatory response by significantly decreasing in 6 h the mRNA expression of IL-1 $\alpha$ , IL-6 and IL-8. All the scaffold types in A549 cells, but in particular the aligned composite ones, enhanced the expression of TGF- $\beta$  and HBD-2, the latter involved in innate immune response. The ZnO/P(VDF-TrFE) electrospun fiber meshes hindered the biofilm formation by *S. aureus* and *P. aeruginosa* and the cell/scaffold constructs were able to impede *S. aureus* adhesion and *S. aureus* and *P. aeruginosa* invasiveness, independently of the scaffold type. The composite scaffolds showed appropriate mechanical properties, with an elongation at break in line with lung's and the possibility to tune the elastic modulus in the range of alveolar walls and fibers. Finally, the fabricated scaffolds also showed good piezoelectricity, which is a feature found in elastic and collagen fibers, the main pulmonary ECM molecules. Even though further studies are necessary to understand the possible physiological roles of piezoelectric materials in lung regeneration and repair, as well as the gas exchange capacity and the mechanobiology of ZnO/P(VDF-TrFE) fiber meshes, these composites have many valuable properties that can match the goal of designing an optimal biomaterial for airway tissue engineering. This includes sufficient cytocompatibility, tunable mechanical properties, good piezoelectricity, strong immunomodulatory properties and good antimicrobial function in particular against *S. aureus*, and in a lesser amount also against *P. aeruginosa*. In conclusion, ZnO/P(VDF-TrFE) fiber meshes developed in this study are promising materials for lung repair and regeneration.

### **Acknowledgements**

NANOSPARKS Project (MISTI; MIT-UNIFI program 2017) is gratefully acknowledged for funding this study. CISUP - Centre for Instrumentation Sharing - University of Pisa is acknowledged for SEM analysis. The authors would like to thank Delfo D'Alessandro and Dr. Stylianos Korasidis, University of Pisa, for technical support to biological characterization and design advices led by expertise in thoracic surgery, respectively.

## References

1. Tebyanian, H., Karami, A., Nourani, M.R., Motavallian, E., Barkhordari, A., Yazdani, M., et al. Lung tissue engineering: An update. *J Cell Physiol* **234**, 19256, 2019.
2. Kovacs, E.J., Boe, D.M., Boule, L.A., and Curtis, B.J. Inflammaging and the Lung. *Clin Geriatr Med*. Nov **33**, 459, 2017.
3. Prakash, Y. S., Tschumperlin, D. J., and Stenmark, K. R. Coming to terms with tissue engineering and regenerative medicine in the lung. *Am J Physiol Lung Cell Mol Physiol*. **309**, L625, 2015.
4. Azimi, B., Milazzo, M., Lazzeri, A., Berrettini, S., Uddin, M.J., Qin, Z., et al. Electrospinning Piezoelectric Fibers for Biocompatible Devices. *Adv Healthc Mater* **9**, 1901287, 2020.
5. Fukada, E. Mechanical deformation and electrical polarization in biological substances. *Biorheology* **5**, 199, 1986.
6. Shamos, M.H. and Lavine, L.S. Piezoelectricity as a fundamental property of biological tissues. *Nature* **213**, 267, 1967.
7. Chen-Glasser, M., Li, P., Ryu, J., and Hong, S. Piezoelectric Materials for Medical Applications, in: Vassiliadis, S.G., and Matsouka, D. Piezoelectricity-Organic and Inorganic Materials and Applications. IntechOpen., 2018, pp.125-145.
8. Kholkin, A., Amdursky, N., Bdikin, I., Gazit, E., and Rosenman, G. Strong piezoelectricity in bioinspired peptide nanotubes. *ACS nano* **4**, 610, 2010.
9. Jiang, P., Yan, F., Nasr Esfahani, E., Xie, S., Zou, D., Liu, X., et al., Electromechanical coupling of murine lung tissues probed by piezoresponse force microscopy. *ACS Biomater Sci Eng* **3**, 1827, 2017.
10. Link, P.A., and Heise, R.L. Pulmonary tissue engineering. In: Hasan, A. Tissue Engineering for Artificial Organs: Regenerative Medicine, Smart Diagnostics and Personalized Medicine. John Wiley & Sons, 2017, pp. 389-413.

11. Nichols, J.E. and Cortiella, J. Engineering of a complex organ: progress toward development of a tissue-engineered lung. *Proc Am Thorac Soc* **5**, 723, 2008.
12. Mota, C., Danti, S., D'Alessandro, D., Trombi, L., Ricci, C., Puppi, D., Dinucci, D., Milazzo, M., Stefanini, C., Chiellini, F., Moroni, L., Berrettini, S. Multiscale fabrication of biomimetic scaffolds for tympanic membrane tissue engineering, *Biofabrication* **7**, 025005, 2015.
13. Kim, K.J., Reynolds, N.M., and Hsu, S.L. Spectroscopic analysis of the crystalline and amorphous phases in a vinylidene fluoride/trifluoroethylene copolymer. *Macromolecules* **22**, 4395, 1989.
14. Kim, K.J. and Kim, G.B. Curie transition, ferroelectric crystal structure and ferroelectricity of a VDF/TrFE (7525) copolymer: 2. The effect of poling on Curie transition and ferroelectric crystal structure. *Polymer* **38**, 4881, 1997.
15. Kim, J., Lee, J.H., Ryu, H., Lee J., Khan, U., Kim, H., et al. High-Performance Piezoelectric, Pyroelectric, and Triboelectric Nanogenerators Based on P (VDF-TrFE) with Controlled Crystallinity and Dipole Alignment. *Adv. Funct. Mater* **27**, 1700702, 2017.
16. Sorayani Bafqi, M.S., Sadeghi, A., Latifi, M., and Bagherzadeh, R. Design and fabrication of a piezoelectric out-put evaluation system for sensitivity measurements of fibrous sensors and actuators. *J Ind Text*, 1528083719867443, 2019.
17. Tashiro, K., Itoh, Y., Kobayashi, M., and Tadokoro, H. Polarized Raman spectra and LO-TO splitting of poly (vinylidene fluoride) crystal form I. *Macromolecules* **18**, 2600, 1985.
18. Bachmann, M. and J. Koenig, Vibrational analysis of phase III of poly (vinylidene fluoride). *The J Che Phys* **74**, 5896, 1981.
19. Ferrone, E., Araneo, R., Notargiacomo, A., Pea, M., and Rinaldi, A. ZnO Nanostructures and electrospun ZnO–polymeric hybrid nanomaterials in biomedical, health, and sustainability applications. *Nanomaterials* **9**, 1449, 2019.

20. Ribeiro, C., Sencadas, V., Correia, D. M., and Lanceros-Méndez, S. Piezoelectric polymers as biomaterials for tissue engineering applications. *Colloid Surface B* **136**, 46, 2015.
21. Sorayani Bafqi, M.S., Bagherzadeh, R., and Latifi, M. Nanofiber alignment tuning: An engineering design tool in fabricating wearable power harvesting devices. *J Ind Text* **47**, 535, 2017.
22. Danti, S., Azimi, B., Candito, M., Fusco, A., Sorayani Bafqi, M.S, Ricci, C., et al. Lithium niobate nanoparticles as biofunctional interface material for inner ear devices. *Biointerphases* **15**(3), 031004, 2020.
23. Balestrini, J.L., and Niklason, L.E. Extracellular matrix as a driver for lung regeneration. *Ann Biomed Eng* **43**, 568, 2015.
24. Pham, Q.P., Sharma, U., Mikos, A.G. Electrospinning of polymeric nanofibers for tissue engineering applications: a review. *Tissue Eng* **12**, 1197, 2006.
25. Paynter, R. W., and Ratner, B. D. *Surface and Interfacial Aspects of Biomedical Polymers* (2<sup>nd</sup> ed.). New York, NY: Springer, 1985.
26. De la Ossa, J.G., Felice, F., Azimi, B., Salsano, J.E., Digiacomo, M., Macchia, M, et al. Waste Autochthonous Tuscan Olive Leaves (*Olea europaea* var. *Olivastra seggianese*) as Antioxidant Source for Biomedicine. *Int J Mol Sci*, **20**, 5918, 2019.
27. Carroll, R.G., Pulmonary System, in: Carroll, R. Elsevier's Integrated Physiology, 2007, pp: 99-115.
28. Yan, J., Qiang, L., Gao, Y., Cui, X., Zhou, H., Zhong, S., et al. Effect of fiber alignment in electrospun scaffolds on keratocytes and corneal epithelial cells behavior. *J Biomed Mater Res A* **100**, 527, 2012.
29. Augustine, R., Malik, H.N., Singhal, D.K., Mukherjee, A., Malakar, D., Kalarikkal, N., et al. Electrospun polycaprolactone/ZnO nanocomposite membranes as biomaterials with antibacterial and cell adhesion properties. *J Polym Res* **21**, 347, 2014.

30. Liang, S., Xiao, K., Mo, Y., and Huang, X. A novel ZnO nanoparticle blended polyvinylidene fluoride membrane for anti-irreversible fouling. *J. Membr. Sci* **394**, 184, 2012.
31. Sorayani Bafqi, M.S., Bagherzadeh, R., and Latifi, M. Fabrication of composite PVDF-ZnO nanofiber mats by electrospinning for energy scavenging application with enhanced efficiency. *J. Polym. Res.* **22**, 130, 2015.
32. Leong, M.F., Chian, K.S., Mhaisalkar, P.S., Ong, W.F., and Ratner, B.D., Effect of electrospun poly(D,L-lactide) fibrous scaffold with nanoporous surface on attachment of porcine esophageal epithelial cells and protein adsorption. *Biomed Mater Res* **89A**, 1040, 2009.
33. Scheirs, J. *Modern Fluoropolymers*. New York, NY: Wiley, 1997.
34. Jawde, S.B., Takahashi, A., Bates, J.H.T., and Suki, B. An analytical model for estimating alveolar wall elastic moduli from lung tissue uniaxial stress-strain curves. *Front. Physiol* **11**, 121, 2020
35. Nuraje, N., Khan, W.S., Lei, Y., Ceylanb, M., and Asmatulu, R. Superhydrophobic electrospun nanofibers. *J. Mater. Chem. A* **1**, 1929, 2013.
36. Spasova, M., Manolova, N., Markova, N., and Rashkov, I. Tuning the Properties of PVDF or PVDF-HFP Fibrous Materials Decorated with ZnO Nanoparticles by Applying Electrospinning Alone or in Conjunction with Electrospraying, *Fiber Polym* **18**, 649, 2017.
37. Ahtzaz, S., and Nasir, M. A study on the effect of zinc oxide and zinc peroxide nanoparticles to enhance angiogenesis-pro-angiogenic grafts for tissue regeneration applications. *Mater. Des* **132**, 409, 2017.
38. Ponnamma, D., and Cabibihan, J.J. Synthesis, optimization and applications of ZnO/polymer nanocomposites. *Mater. Sci. Eng. C* **98**, 1210, 2019.
39. Fujiwara, Y., and Kaji, T. Zinc potentiates the stimulation by basic and acidic fibroblast growth factors on the proliferation of cultured vascular smooth muscle cells. *Res Commun Mol Pathol Pharmacol* **97**, 95, 1997.

40. Paez-Cortez, J., Krishnan, R., Arno, A., Aven, L., Ram-Mohan, S., Kruti, R. et al. A new approach for the study of lung smooth muscle phenotypes and its application in a murine model of allergic airway inflammation. *PLoS ONE* **8**, 74469, 2013.
41. Cigana, C., Bianconi, I., Baldan, R., De Simone, M., Riva, C., Sipione, B, et al. *Staphylococcus aureus* impacts *pseudomonas aeruginosa* chronic respiratory disease in murine models. *J Infect Dis.* **217**, 933, 2018.
42. Donnarumma, G., Paoletti, I., Fusco, A., Perfetto, B., Buommino, E., de Gregorio, V., et al.  $\beta$ -Defensins: Work in Progress. *Adv Exp Med Biol* **901**, 59, 2016.
43. Dinarello, C.A. Interleukin-1. *Cytokine Growth Factor Rev* **8**, 253, 1997.
44. Arnold, R., Humbert, B., Werchau, H., Gallati, H., and König, W. Interleukin-8, interleukin-6, and soluble tumour necrosis factor receptor type I release from a human pulmonary epithelial cell line (A549) exposed to respiratory syncytial virus. *Immunology* **82**, 126, 1994.
45. Yoshimura, A., Wakabayashi, Y., and Mori, T. Cellular and molecular basis for the regulation of inflammation by TGF- $\beta$ . *J. Biochem* **147**, 781, 2010.
46. Aghasafari, P., George, U., and Pidaparti, R. A review of inflammatory mechanism in airway diseases *Inflamm Res* **68**, 59, 2019.
47. Persano, L., Dagdeviren, C., Su, Y., Zhang, Y., Girardo, S., Pisignano, D., et al. High performance piezoelectric devices based on aligned arrays of nanofibers of poly (vinylidene fluoride-co-trifluoroethylene). *Nat. commun* **4**, 1633, 2013.
48. Mota, C., Labardi, M., Trombi, L., Astolfi, L., D'Acunto, M., Puppi, D., et al. Design, fabrication and characterization of composite piezoelectric ultrafine fibers for cochlear stimulation. *Mater. Des* **122**, 206, 2017.
49. Augustine, R., Dan, P., Sosnik, A., Kalarikkal, N., Tran, N., Vincent, B., Thomas, S., Menu, P., Rouxel, D. Electrospun poly(vinylidene fluoride-trifluoroethylene)/zinc oxide nanocomposite tissue engineering scaffolds with enhanced cell adhesion and blood vessel formation. *Nano Res.* **10**, 3358–3376, 2017.

## Figure legends

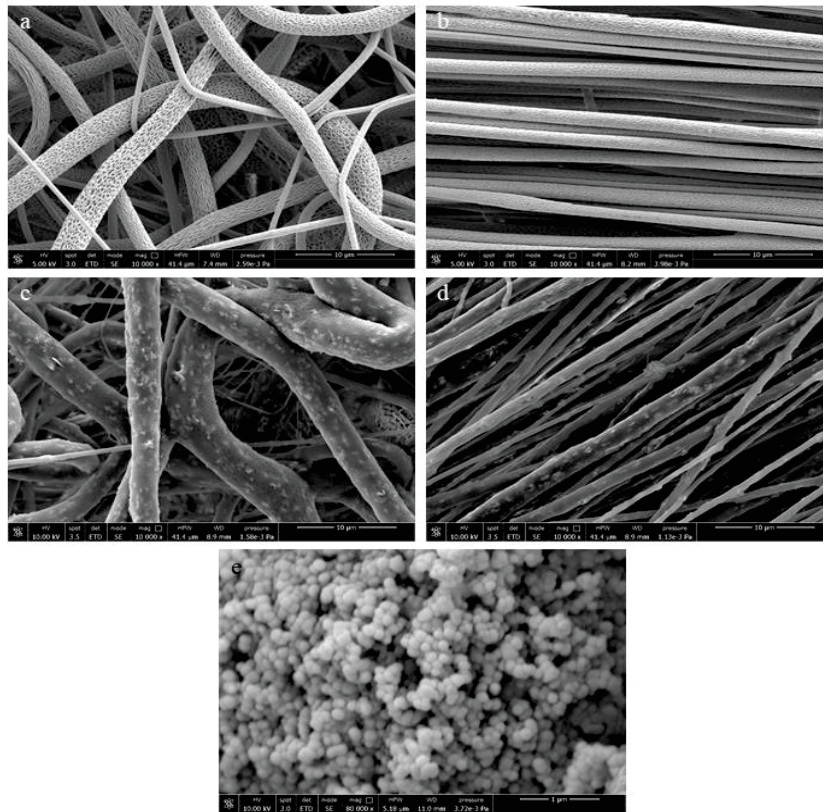


**Figure 1.** SEM micrographs showing: (a-d) ZnO/P(VDF-TrFE) fiber meshes, specifically, (a,b) 0/100 (w/w%) and (c,d) 20/80 (w/w%), produced at (a,c) 500 rpm and (b,d) 4000 rpm; and, (d) ZnO nanopowder, as observable in inserts in (c,d).

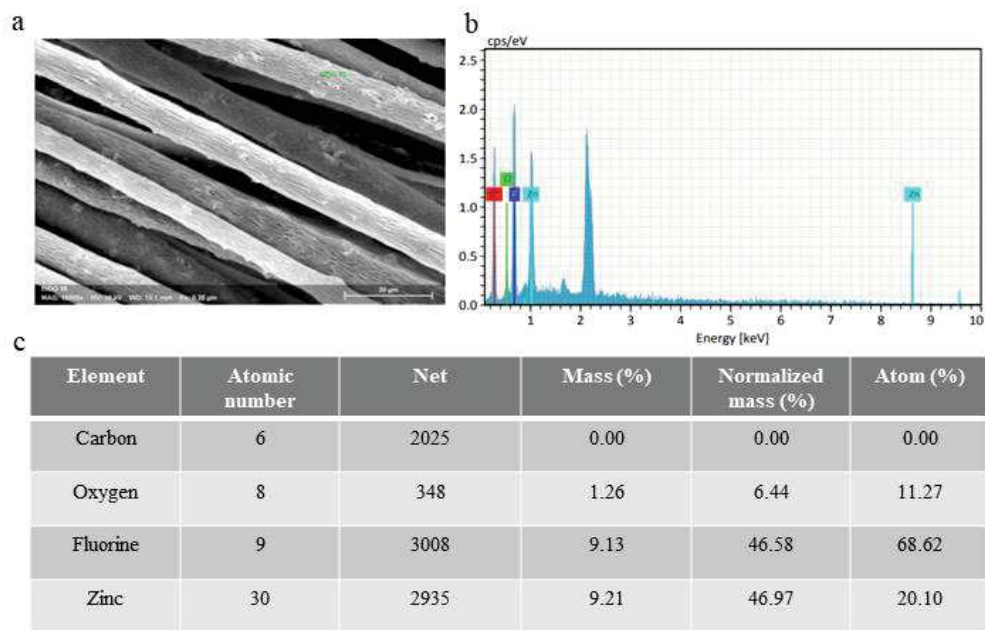


**Figure 2.** EDXS results of 20/80 (w/w%) ZnO/P(VDF-TrFE) displaying: (a) the selected area in a SEM micrograph, (b) the corresponding element analysis showing the peaks of C, F, Zn and O, and (c) the associated quantitative table.

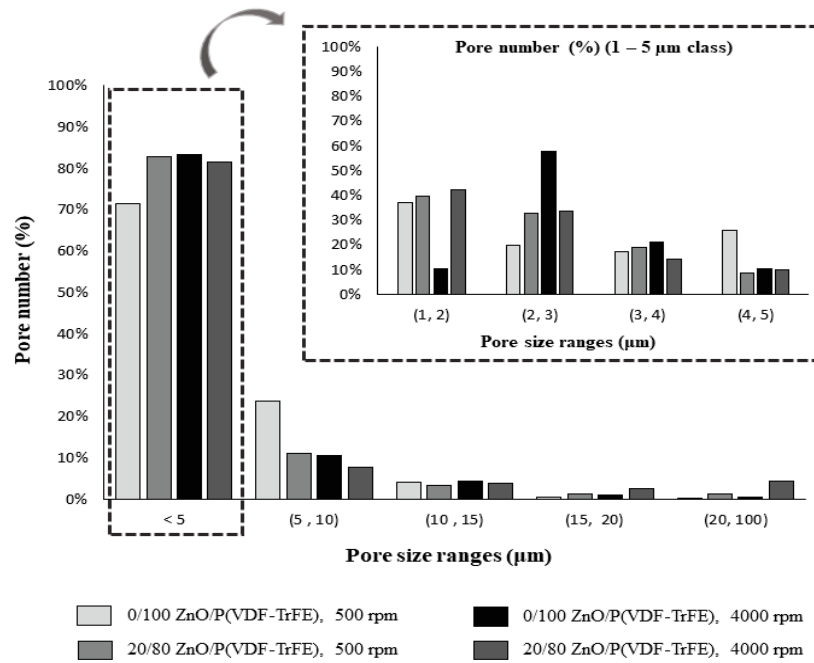


**Figure 3.** Pore size distribution for different ZnO/P(VDF-TrFE) fiber meshes evaluated in the range 1-100 µm according to different diameter classes; distribution of pores with diameters ≤ 5 µm is shown in the lens.

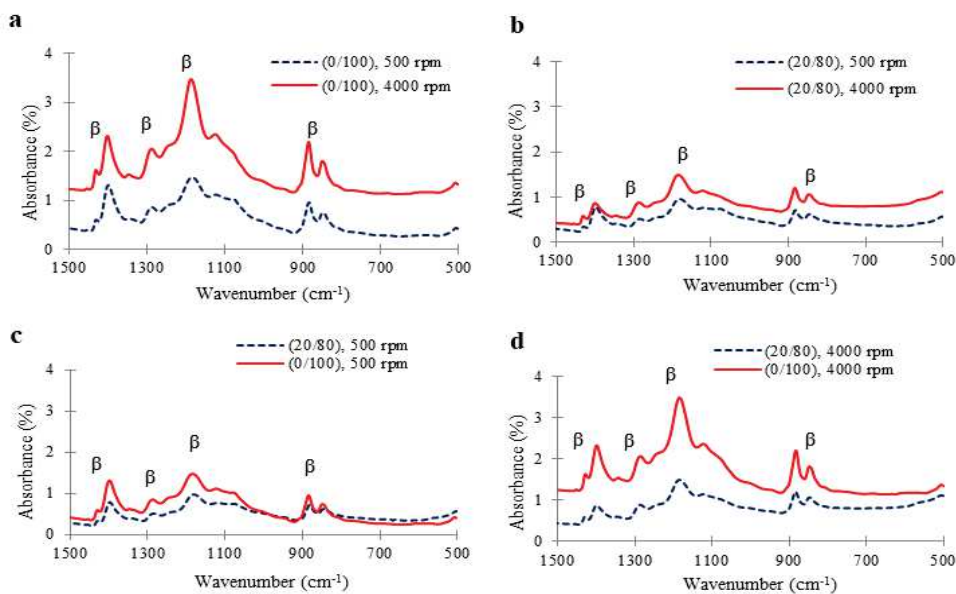


**Figure 4.** Comparisons of FTIR spectra of ZnO/P(VDF-TrFE) fiber meshes produced at different collector velocities showing the peaks associated with crystalline  $\beta$  phases typical of the polymer: (a) 0/100 (w/w%), 500 rpm versus 4000 rpm; (b) 20/80 (w/w%), 500 rpm versus 4000 rpm; (c) 500 rpm, 0/100 versus 20/80 (w/w%); (d) 500 rpm, 0/100 versus 20/80 (w/w%).

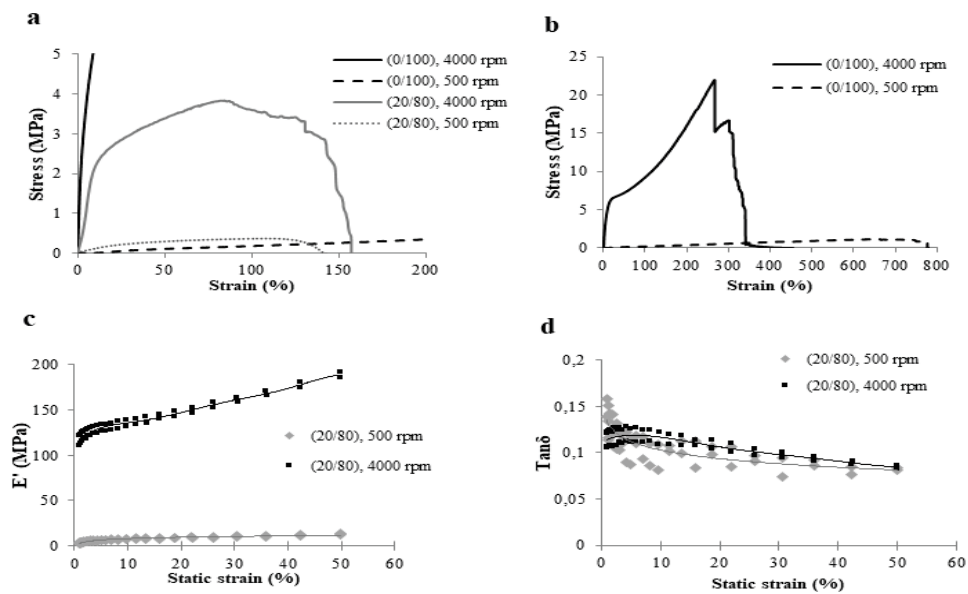


**Figure 5.** Mechanical characterization of ZnO/P(VDF-TrFE) scaffolds in tensile mode: (a, b) tensile tests showing stress-strain curves of (a) all the scaffold types within a restricted region of observation, namely 0-5 MPa stress versus 0%-200% strain, (b) (0/100) ZnO/P(VDF-TrFE) scaffolds in the entire range namely 0-25 MPa stress versus 0%-800% strain; (c-d) DMA analysis of the (20/80) ZnO/P(VDF-TrFE) showing the complex modulus parameters, namely (c) storage modulus ( $E'$ ) and (d) loss tangent ( $\tan\delta$ ).

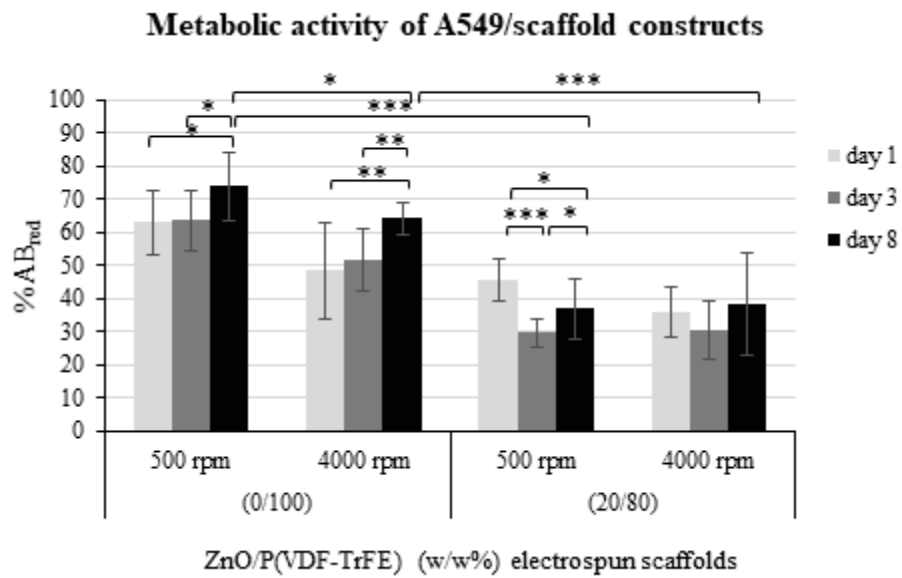


**Figure 6.** Bar graph showing the metabolic activity (as reduction percent of alamarBlue dye; %AB<sub>red</sub>) of A549 lung alveolar cells cultured on (0/100) and (20/80) (w/w%) ZnO/P(VDF-TrFE) fiber meshes produced at 500 rpm and 4000 rpm up to 8 days. Data are given as mean  $\pm$  SD ( \*  $p < 0.5$ , \*\*  $p < 0.01$ , and \*\*\*  $p < 0.001$ ).

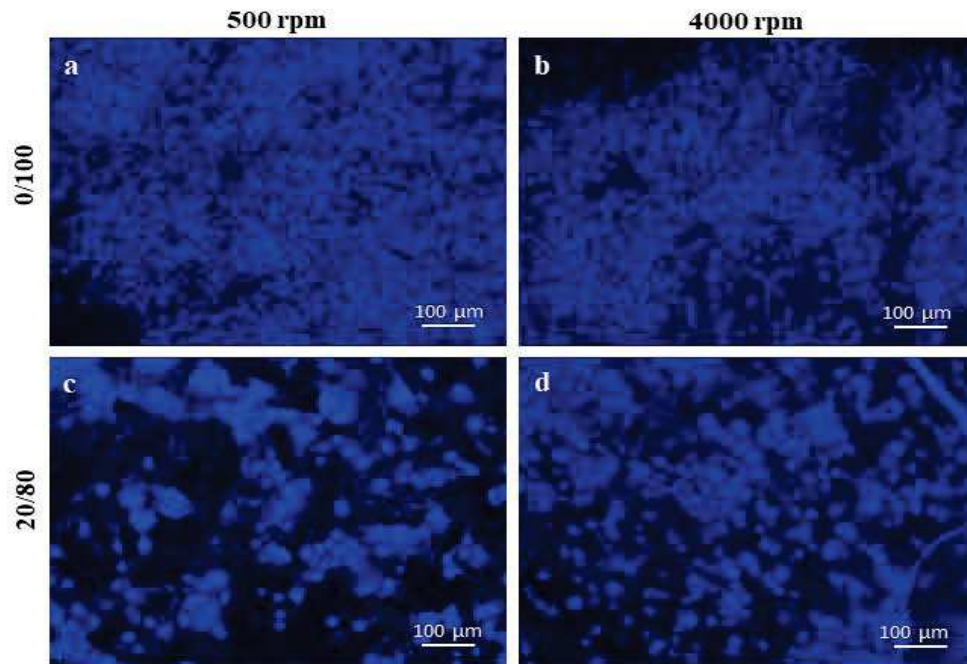


**Figure 7.** DAPI staining under fluorescence microscopy on alveolar cell/ZnO/P(VDF-TrFE) constructs after 8 days in culture showing cell nuclei in blue on the top surface of the scaffolds: (a, b) (0/100) and (c, d) (20/80) ZnO/P(VDF-TrFE) scaffolds, fabricated at (a, c) 500 rpm and (b, d) 4000 rpm collector velocities, thus resulting in random and aligned fibers, respectively. Scale bar = 100 μm; original magnification = 100×.

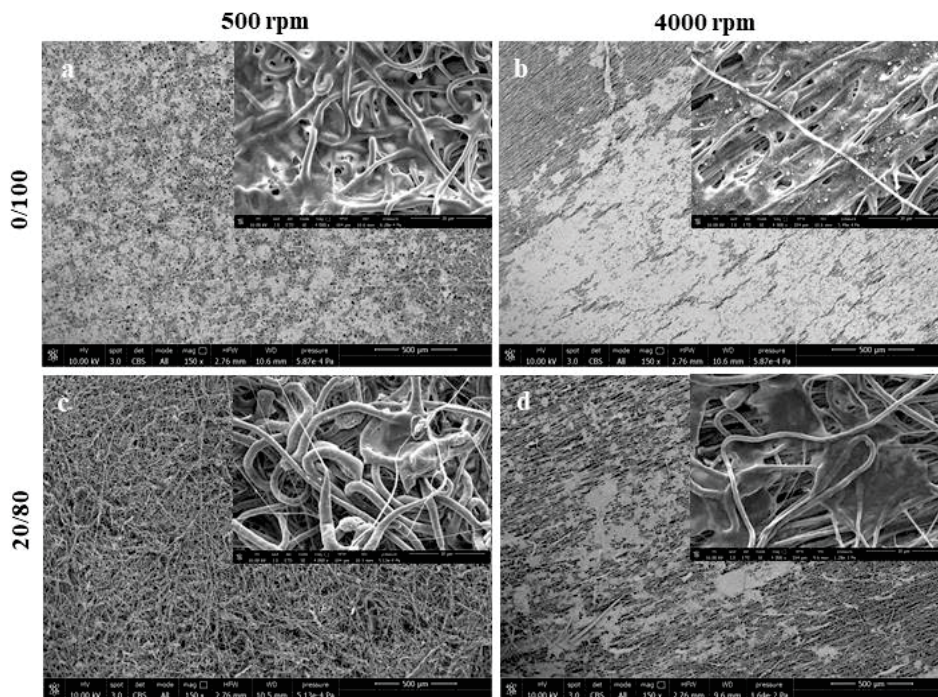


**Figure 8.** SEM analysis on alveolar cell/ZnO/P(VDF-TrFE) constructs after 8 days in culture showing cells on the top surface of the scaffolds: (a, b) (0/100) and (c, d) (20/80) ZnO/P(VDF-TrFE) scaffolds, fabricated at (a, c) 500 rpm and (b, d) 4000 rpm collector velocities, thus resulting in random and aligned fibers, respectively. Insets in each micrograph image display zoomed-in areas showing single or grouped cells adhered to the fibers.

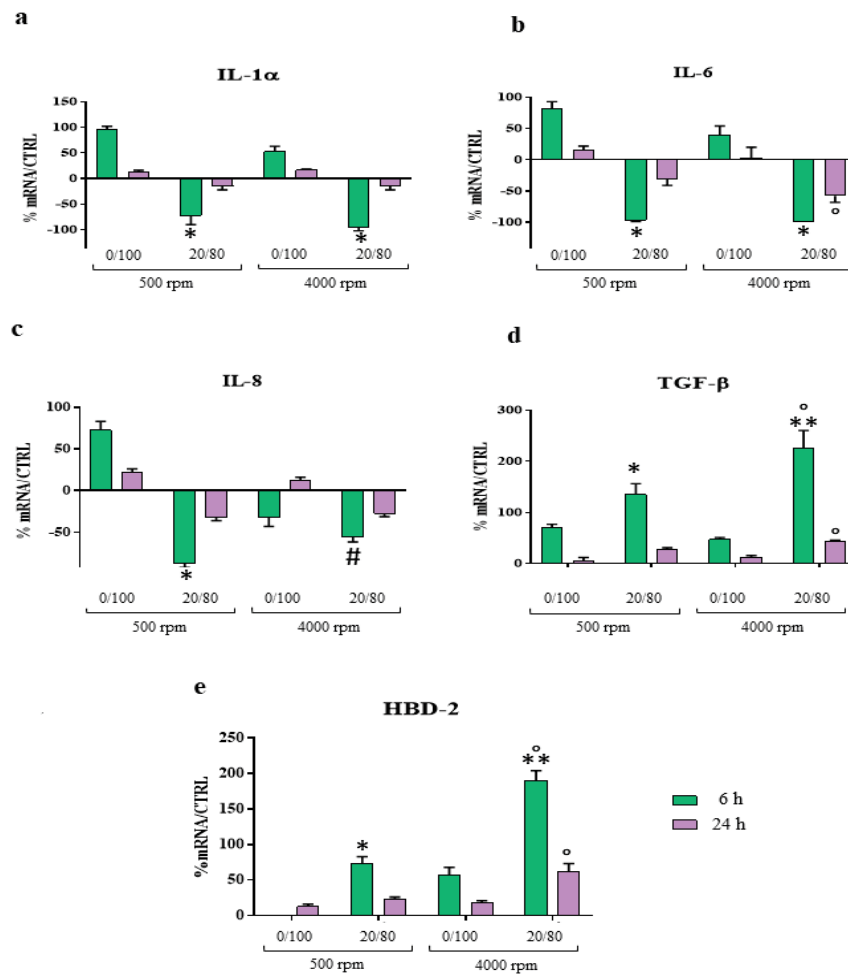


**Figure 9.** Bar graph showing chemokine expression via RT-PCR by A549 cells cultured for 6 h and 24 h in contact with plain and composite ZnO/P(VDF-TrFE) electrospun fiber scaffolds collected at 500 rpm and 4000 rpm respect to A549 cell basal conditions (2D culture): (a) IL1- $\alpha$ ; (b) IL-6; (c) IL-8; (d) TGF- $\beta$ ; and (e) HBD-2. Data are expressed as mean  $\pm$  SD; \*  $p < 0.01$  vs. (0/100) counterpart; \*\*  $p < 0.0001$  vs. (0/100) counterpart; #  $p < 0.01$  vs. (0/100) counterpart; <sup>o</sup>  $p < 0.001$  vs. all.

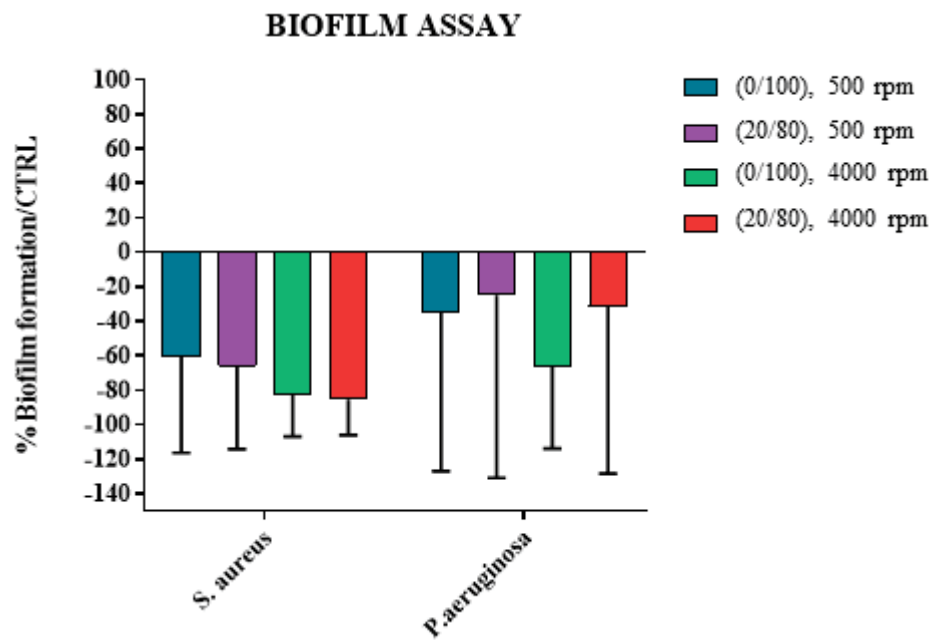


**Figure 10.** Bar graph showing the results of the biofilm formation assay conducted using *S. aureus* and *P. aeruginosa* on plain and composite ZnO/P(VDF-TrFE) electrospun fiber scaffolds collected at 500 rpm and 4000 rpm for 24 h. Data are expressed as mean  $\pm$  SD.

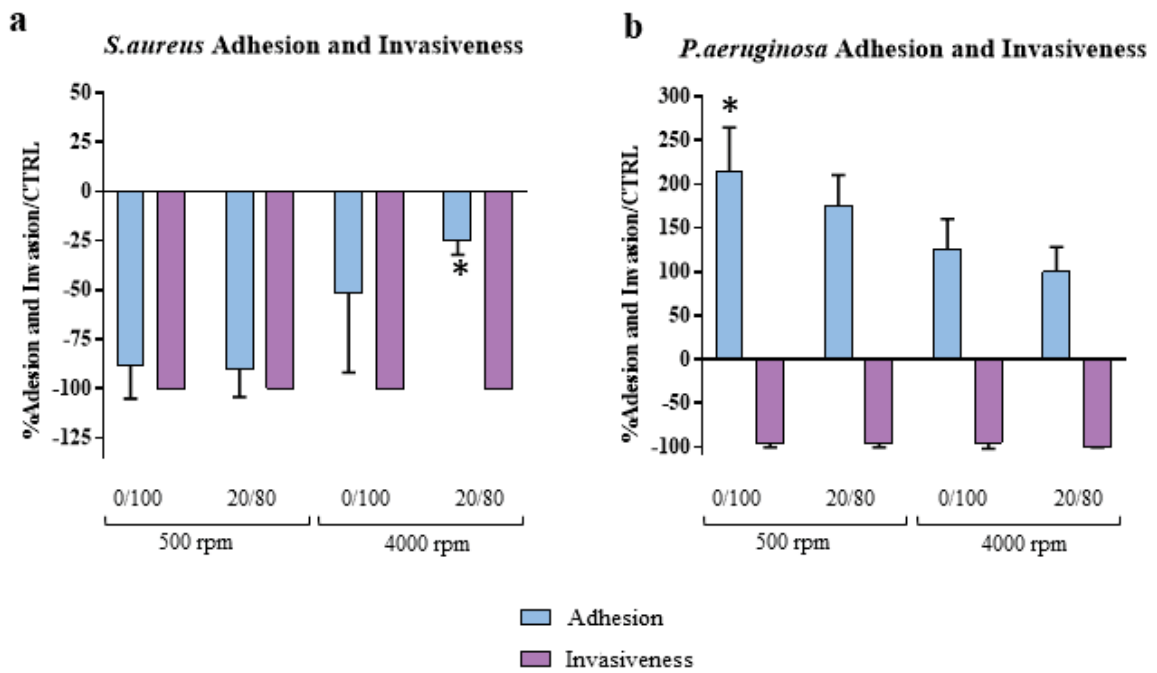


**Figure 11.** Bar graph showing the results of the adhesion and invasiveness assays conducted after 24 h on plain and composite ZnO/P(VDF-TrFE) electrospun fiber scaffolds collected at 500 rpm and 4000 rpm, using (a) *S. aureus*, and (b) *P. aeruginosa*. Data are expressed as mean  $\pm$  SD; \*  $p < 0.001$ .

**Table 1.** RT-PCR details, including gene, primer sequences, operational conditions and product size.

| Gene          | Primers sequence  | Conditions  | Product size (bp) |
|---------------|---|---|-------------------|
| IL-1 $\alpha$ | 5'-CATGTCAAATTTCACTGCTTCATCC -3'<br>5'-GTCTCTGAATCAGAAATCCTTCTATC -3'   | 5 s at 95°C, 8 s at 55°C, 17 s at 72°C for 45 cycles  | 421               |
| IL-1 $\beta$  | 5'-GCATCCAGCTACGAATCTCC-3'<br>5'-CCACATTCAGCACAGGACTC-3'                | 5 s at 95°C, 14 s at 58°C, 28 s at 72°C for 40 cycles | 708               |
| IL-6          | 5'-ATGAACTCCTTCTCCACAAGCGC-3'<br>5'-GAAGAGCCCTCAGGCTGGACTG-3'           | 5 s at 95°C, 13 s at 56°C, 25 at 72°C for 40 cycles   | 628               |
| IL-8          | 5'-ATGACTTCCAAGCTGGCCGTG-3'<br>5'-TGAATTCTCAGCCCTCTTCAAAAATTCTC-3'      | 5 s at 94°C, 6 s at 55°C, 12 s at 72°C for 40 cycles  | 297               |
| TNF- $\alpha$ | 5'-CAGAGGGAAGAGTCCCCAG -3'<br>5'-CCTTGGTCTGGTAGGAGACG -3'               | 5 s at 95°C, 6 s at 57°C, 13 s at 72°C for 40 cycles  | 324               |
| TGF- $\beta$  | 5'-CCGACTACTACCCAAGGAGGTCAC-3'<br>5'-AGGCCGGTTCATGCCATGAATGGTG-3'       | 5 s at 94°C, 9 s at 60°C, 18 s at 72°C for 40 cycles  | 439               |
| HBD-2         | 5'-GGATCCATGGGTATAGGCGATCCTGTTA-3'<br>5'-AAGCTTCTCTGATGAGGGAGCCCTTCT-3' | 5'' at 94°C, 6'' at 63°C, 10'' at 72°C for 50 cycles  | 198               |

**Table 2.** ZnO/P(VDF-TrFE) fiber diameter ( $n = 100$ ) and fiber mesh porosity in different compositions (0/100 and 20/80 w/w%) and process conditions (500 rpm and 4000 rpm). Data are expressed as mean  $\pm$  standard deviation, statistical significance is considered for  $p < 0.05$ ; n.s. is non-significant.

| Sample type (#) | ZnO/P(VDF-TrFE) (w/w%) | Collector speed (rpm) | Fiber diameter ( $\mu\text{m}$ ) | Statistical significance ( $p$ ) | Porosity (%) | Statistical significance ( $p$ ) |
|-----------------|------------------------|-----------------------|----------------------------------|----------------------------------|--------------|----------------------------------|
| 1               | 0/100                  | 500                   | 1.86 $\pm$ 0.48                  | $2 \cdot 10^{-21}$ (vs. # 2)     | 94% $\pm$ 1% | 0.002 (vs. # 2)                  |
| 2               | 0/100                  | 4000                  | 1.27 $\pm$ 0.20                  | $8 \cdot 10^{-8}$ (vs. # 4)      | 85% $\pm$ 2% | 0.410 (vs. # 4)                  |
| 3               | 20/80                  | 500                   | 2.43 $\pm$ 0.76                  | $6 \cdot 10^{-10}$ (vs. # 1)     | 92% $\pm$ 5% | n.s. (vs. # 1)                   |
| 4               | 20/80                  | 4000                  | 1.62 $\pm$ 0.58                  | $1 \cdot 10^{-14}$ (vs. # 3)     | 89% $\pm$ 7% | n.s. (vs. # 3)                   |

**Table 3.** DSC and FTIR data for ZnO/P(VDF-TrFE) fiber meshes in different composition (0/100 and 20/80 w/w%) and process conditions (500 rpm and 4000 rpm).

| ZnO/P(VDF-TrFE)<br>(w/w%) | Collector<br>speed (rpm) | Melting<br>Temperature<br>(°C) | Melting<br>Enthalpy<br>(J·g <sup>-1</sup> ) | Xc<br>(%) | F(β)<br>(%) |
|---------------------------|--------------------------|--------------------------------|---|-----------|-------------|
| 0/100                     | 500                      | 151.2                          | 27.8  | 30.39     | 81.61       |
| 0/100                     | 4000                     | 152.2                          | 29.43                                       | 32.18     | 90.44       |
| 20/80                     | 500                      | 145.1                          | 24.88                                       | 27.20     | 70.48       |
| 20/80                     | 4000                     | 146.3                          | 25.28                                       | 27.65     | 78.42       |

**Table 4.** Piezoelectric properties of ZnO/P(VDF-TrFE) pure and composite fibers electrospun at different collector velocities. All the tests were performed under a 2.12 N applied load. CV is the coefficient of variation.

| ZnO/P(VDF-TrFE) (w/w %) | Collector Velocity (rpm) | $V_{out}$ (mV) | Sensitivity (mV/N) | Thickness ( $\mu\text{m}$ ) | Normalized Sensitivity (mV/N $\cdot\mu\text{m}$ ) | CV (%) |
|-------------------------|--------------------------|----------------|--------------------|-----------------------------|---|--------|
| 0/100                   | 500                      | $45 \pm 5$     | 21.22              | 40                          | 0.53  | 11.05  |
| 0/100                   | 4000                     | $80 \pm 1$     | 37.73              | 40                          | 0.94  | 0.99   |
| 20/80                   | 500                      | $80 \pm 1$     | 37.73              | 40                          | 0.94  | 1.21   |
| 20/80                   | 4000                     | $90 \pm 1$     | 42.45              | 30                          | 1.41  | 0.88   |